Seismological and geological analysis of mine collapses in Northeast Estonia

Bachelor thesis

Student: Trinity Jõgisalu
Student code: 222352LARB
Supervisor: Heidi Soosalu, Department of Geology, Senior Lecturer
Study program: Earth Systems, Climate and Technologies

Tallinn 2025

Declaration

I hereby declare that I have written this thesis independently and the thesis has not previously been submitted for defence. All works and major viewpoints of the other authors, data from sources of literature and elsewhere used for writing this paper have been properly cited.

Author: Trinity Jõgisalu

The thesis complies with the requirements for bachelor's theses

Supervisor: Heidi Soosalu

Table of Contents

Declaration 1
Annotatsioon 4
Abstract 5
List of Figures 6
List of Tables 7
1. Introduction 8
2. Oil shale in Estonia 9
2.1. Geological conditions 10
2.2. Hydrogeology 11
2.3. Mining conditions 12
2.4. Impact of mining 14
2.5. Study of collapse areas 20
3. Seismology 21
3.1. Seismicity in mining 21
3.2. Destructive forces of a collapse 22
4. Analysis of seismological data 24
4.1. Noise and filters 24
4.2. Signal stacking 25
4.3. Comparison of seismic events 25
4.3.1. Earthquake 25
4.3.2. Explosion at an open cast mine 27
4.3.3. Mine collapse 29
5. Methodology 32
5.1. Event isolation and seismogram clipping 32
5.2. Signal filtration 33
5.3. Stacking 34
6. Results 37
6.1. Time related factors 37
6.2. Meteorological conditions 41
6.3. Location 42
7. Conclusions and Discussion 45
Summary 46

Acknowledgements 47

References 48

Appendix 1. An example Python code used to plot seismic data 51

Appendix 2. An example of an output file of the routine seismic analysis of Estonian events, featuring the collapse in the Estonia mine in December 2023 (from Soosalu, 2024). 52

Appendix 3. A map with all collapses and where they occurred in the oil shale mines. Shown in Figure 26 and in a separate file on a magnified scale. 53

Kirde-Eesti kaevandusvaringute seismiline ja geoloogiline analüüs

Annotatsioon

Käesolev töös uuritakse Kirde-Eesti põlevkivikaevandustes toimunud maa-aluseid varinguid, analüüsides aastatel 2008–2023 nende kohta registreeritud seismilisi andmeid. Eesmärk on tuvastada korduvaid mustreid ja neid soodustavaid tegureid, mis võivad viia struktuuriliste riketeni nii aktiivses kaevanduses kui ka piirkondades, mis on aktiivsest tööfaasist möödas. Soome ja Eesti seismojaamade salvestisi töödeldi ja analüüsiti, et eristada varingusignaale teistest erinevat tüüpi seismilistest sündmustest, nagu maavärinad ja lõhkamised pealmaakaevandustes. Filtreerimise, seismogrammide analüüsi ja signaalide summeerimise abil näitab uuring, et Eesti põlevikivkaevanduste varingud tekitavad unikaalseid seismilisi signaale, mida iseloomustavad madalad sagedused ja pikk signaali kestus.

Sündmuste ajalise jaotuse analüüs näitab, et varingud olid uuringuperioodi vältel sagedasemad talvel ja varakevadel, ning et neid toimus eriti öisel ajal. Need mustrid viitavad seosele maapõue pingevälja muutvate keskkonnatingimustega, nagu külmumis-sulamistsüklid, lume sulamine ja põhjavee infiltratsioon ning samuti kaevetööde ajutiste peatumistega. Geograafiliselt näivad varingud olevat kooskõlas teadaolevate geoloogiliste tunnustega, nagu rikked ja karstivööndid, mis rõhutab geoloogiliste tingimuste rolli.

Abstract

The topic of this thesis is underground collapse events in the oil shale mines of Ida-Viru County, northeastern Estonia, through the analysis of seismological data recorded between 2008 and 2023. The aim is to identify recurring patterns and contributing factors that may lead to structural failures within both active mines and areas where no active stages of operations are ongoing. Data from Finnish and Estonian seismic stations were processed and analysed to distinguish collapse signals from other seismic events, such as earthquakes and explosions in quarries or open cast mines. Using filtering techniques, waveform analysis, and signal stacking, the study reveals that mine collapses in Estonian oil shale mines generate uniquely identifiable seismic signals characterized by low-frequency content and prolonged duration.

Analysis of event distribution over time indicates that within the study period collapses were more frequent during winter and early spring, and they took place particularly in the night-time. These patterns suggest a correlation with environmental conditions such as freeze-thaw cycles, snowmelt, and groundwater infiltration, as well as operational pauses that alter the stress state within the mines. Geographically, collapses seem to align with known geological features such as fault structures and karst zones, highlighting the role of geological conditions.

List of Figures

Figure 1. Location of the kukersite deposits within the Baltic Oil Shale Basin in northern Estonia (Dyni, 2006)..... 10
Figure 2. Pandivere Upland (Pandivere kõrgustik, n.d.)..... 12
Figure 3. An outline of room-and-pillar mining (Reinsalu, 2011). 13
Figure 4. Kukersite and limestone layers in the oil shale deposit (Dyni, 2006). 14
Figure 5. Changes of landscape caused by the 2017 collapse in Estonia mine (Soosalu, 2018). 16
Figure 6. A hazardous area caused by the 2017 collapse (Soosalu, 2018)..... 17
Figure 7. A collapse from the year 2008 which caused the frees above it to tilt towards its centre (Soosalu, 2009). 18
Figure 8. A considerably large surface opening above the collapse from 2008 (Soosalu, 2009). 19
Figure 9. Propagation characteristics of seismic waves (Triton et al., 2023). 21
Figure 10. Z-, N- and E-component seismograms of the station VJF for the Väike-Maarja earthquake. 26
Figure 11. Z-component spectrogram of the Väike-Maarja earthquake. 27
Figure 12. Three-component seismograms of the Narva open cast mine explosion at the station PISE. 28
Figure 13. Spectrogram of the Z-component recording of the explosion. 29
Figure 14. Seismograms of the collapse that are strikingly different from the previous events..... 30
Figure 15. Z-component spectrogram of the collapse, presenting the unique low-frequency “tail”... 31
Figure 16. A map of all seismic stations used or considered for data analysis. 33
Figure 17. Unfiltered seismograms of the Z- and E-components of the station EE06..... 34
Figure 18. Comparisons between seismograms of individual events and two-event stacked seismograms..... 36
Figure 19. The 11 collapses over a 16-year period. 38
Figure 20. Distribution of collapses by months..... 39
Figure 21. The distribution of weekdays when collapses have occurred. 39
Figure 22. Times of day when collapses have occurred, in UTC time. 40
Figure 23. Times of day when collapses have occurred, in local EET/EEST time. 40
Figure 24. Number of collapses that took place in each season..... 41
Figure 25. Collapses per km^2 represented by black circles and coloured by event density. 43
Figure 26. An overview of the oil shale mining region under analysis. The map was made using Autodesk Civil 3D..... 44

List of Tables

Table 1. Origin times, locations and magnitudes of the studied mine collapses (Seismic Events, n.d.) 9
Table 2. Locations of all stations used for analysis. Other stations were used for testing but not for conclusions. Coordinates from Soosalu, 2025 and Institute of Seismology, 1980. 32

1. Introduction

This thesis focuses on analysis of seismological data related to underground collapses in the oil shale mines in the Ida-Viru County, northeastern Estonia. Conditions and features that may have contributed to these events are discussed. The seismic data used in this study comprises records collected by Finnish and Estonian seismic stations during the years 2008 to 2023. The primary goal is to determine whether mine collapses occur due to coinciding factors such as mining technology, activity or inactivity of mining operations, time of day, seasonal weather conditions and changes in regional hydrology. Such conditions may attribute to changes in the stress field within the mine chambers, addressing additional pressure on pillars and the roof from different directions. As mining activities already disrupt the natural distribution of stresses between different materials that make up the terrain, only a slight displacement in the rock mass may have the potential to cause powerful collapses with accompanying shockwaves.

Failures of underground structures are hazardous in many ways, both to people and to the environment. Ensuring the safety of workers is a main priority in active mining operations and collapses have the potential to cause serious injury as well as damage operational equipment. Both cases result in the halting of operations which will cost the company both time and profit. Accidents in mines can mean costly repairs for equipment and investigations into the cause of the incident which may also lead to legal repercussions if any violations in safety regulations are discovered. Environmental protection is also important regarding both active and inactive mines. If mining structures fail, the consequences may include unstable surfaces near populated areas, contamination of groundwater, surfacing of toxic gases and a general disruption to the environment. By examining collapses, it is possible to improve the structural integrity of mines as well as the use of mining technology, thus minimizing the risk of future rock burst events and optimizing operational productivity. Considering factors contributing to possible weaknesses in mine chambers greatly aids the planning of safe and efficient mining operations.

The main tasks in this study are to examine collected seismological data, isolate events of interest and learn to analyse and interpret seismograms. Along with presenting the geological conditions and technology used in Estonian oil shale mines, examples of rock burst events from other mines are also presented as well as comparisons about different types of events registered by seismic stations. Conditions attributing to collapses are evaluated to determine whether these events could be predicted and prevented beforehand.

2. Oil shale in Estonia

Collapses that I have analysed have occurred in oil shale mines called Sompa, Viru and Estonia. The number of events is largest in the Estonia mine, which is also the only one of the three that is still in the phase of active mining. Exact locations of the collapses in Estonia have been confirmed by the mining company currently known as Enefit Kaevandused Ltd, while events from the two inactive mines have been estimated based on data recorded by seismic stations. Below is Table 1 that shows the eleven collapses under analysis.

Table 1. Origin times, locations and magnitudes of the studied mine collapses (Seismic Events, n.d.)

YYYY/MM/DD	UTC time	°N	°E	Magnitude	Mine
2008/01/20	23:30	59.241	27.439	1.6	Estonia
2008/07/01	22:44	59.242	27.434	1.8	Estonia
2015/03/06	11:40	59.267	27.359	1.4	Estonia
2015/03/17	15:20	59.257	27.342	1.5	Estonia
2016/03/04	01:23	59.274	27.342	1.5	Viru
2016/03/04	22:45	59.290	27.315	0.9	Viru
2016/06/07	05:01	59.318	27.311	1.3	Sompa
2016/10/24	14:28	59.295	27.307	1.5	Viru
2017/03/16	07:46	59.197	27.336	2.2	Estonia
2021/01/30	23:38	59.253	27.404	1.0	Estonia
2023/12/24	04:53	59.207	27.415	1.6	Estonia

Estonia is located on the East European Platform where the Ordovician, Silurian and Devonian Systems are widespread. Estonian oil shale is present in Ordovician rocks, which are well-exposed in coastal cliffs, riverbanks and limestone quarries. The Ordovician System is divided into the Lower, Middle and Upper Ordovician stages and their corresponding formations. The Ordovician rocks found in Estonia include sandstone, argillite, clays, glauconitic sand- and siltstone, limestone, dolostone and kukersite oil shale. Kukersite is found in the Upper Ordovician Kukruse stages Viivikonna formation and the Middle Ordovician Uhaku stages Kõrgekallas formation (Meidla et al., 2014).

2.1. Geological conditions

The Baltic Oil Shale Basin has an area of around 50,000 km^2 and it is located at the northwestern edge of the East European Sedimentary Platform. The border between the Kukruse and Uhaku stages is considered as the northern boundary of the basin, 5–10 km from the coast of the Gulf of Finland, and it continues for over 100 km until the kukersite layers gradually thin out. The Estonian kukersite deposit takes up most of the western half of the Baltic Oil Shale Basin. Within Estonian borders the deposits north section is located on the Northeast Estonia Plateau, the west section on the Pandivere Upland and the east section on the Alutaguse Lowland. Bedrock starts at an elevation of 30–60 m and reaches an elevation of 100–120 m at the centre of the Pandivere Upland. Bedrock topography of northern Estonia presents ancient valleys that have been eroded into the bedrock and are filled with Quaternary sediments. These ancient valleys also cut into the Estonian oil shale deposit (Kattai et al., 2000).

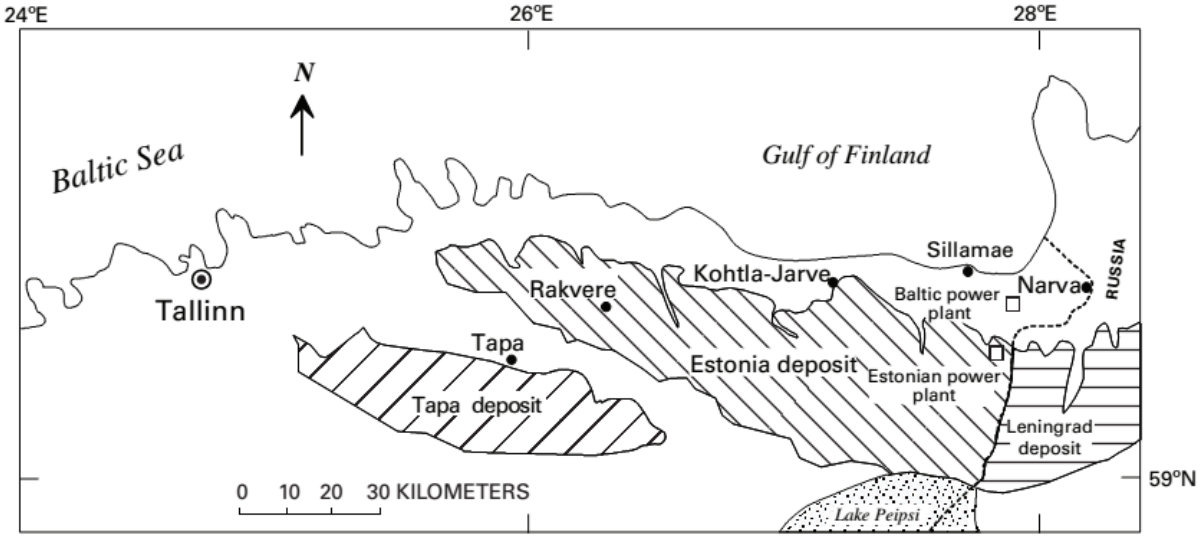

Figure 1. Location of the kukersite deposits within the Baltic Oil Shale Basin in northern Estonia (Dyni, 2006).

The kukersite deposit (Figure 1) is well-studied and largely exploited. It has an organic content up to 65%, a calorific value of 9–11 MJ/kg and yields 22–24% of extractable oil. The shallow depth of 10–90 m of the deposit and an overall horizontal bedding make the mining conditions rather favourable. Before the increase of utilizing renewable energy sources, about 80–85% of mined oil shale was used for energy production while the rest went into the chemical industry (Raudsep, 2008).

The nearly horizontal Lower Palaeozoic sedimentary complex of northeastern Estonia has generally linear fault belts and local structures such as anticlines and depressions. Most fault belts are oriented northeast to southwest but may vary as much as 10° in the northeast direction. These belts divide the oil shale field into blocks that may be vertically shifted 5–25 m relative to each other. Many of the fault belts are estimated to extend at depth through the entire sedimentary complex and may be connected to deep faults in the crystalline basement (Kattai et al., 2000).

Much of northeastern Estonia is located on Silurian and Ordovician rocks where karstification is particularly widespread. Karst formed after the last glaciation 10,000–14,000 years ago and despite

being relatively young, it has ma influenced regional geology and hydrology considerably. The natural development of karst may also be intensified by human activities, such as in areas like Kohtla-Järve where oil shale has been mined for over a century. Tectonically active regions like the Pandivere Upland often have karst zones that coincide with fault zones where pre-existing fractures may have been deepened up to 75 m in depth. Karstified areas complicate mining conditions by increasing ground instability and risk of water contamination (Koit, 2018).

The rocks in and around fault belts are often fractured, cavernous, dolomitized, weathered and have undergone karstification and sulphide mineralization. Fracturing of the useful seam and surrounding rock and karst worsen mining conditions the most. Single tectonic dislocations go through the Ordovician carbonate rock sequence in between the regions linear fault belts. These faults may be closed, open or filled with clay or sandstone. Karst zones are present throughout the entire Ordovician system, occurring both near the surface and deeper in the rock. Surface karst forms funnels and furrows while deep karst follows channels and creates caverns. This type of karst typically has a central leaching zone where oil shale has been replaced by clay with outer edges of fractured rock surrounding it. Clay zones within the karst can be one to tens of meters wide and considering the shattered rock areas can stretch the entire zone up to 200 metres in width. These zones seldom appear separately but rather in groups. According to areal distribution of karst clay to mined oil shale, highest amount (2–4%) was observed in the Viru and Sompa mines. The Estonia mine has a percentage below 1% (Kattai et al., 2000).

2.2. Hydrogeology

The hydrogeological conditions of Estonia's oil shale deposit have mainly been shaped by the slopes of the Pandivere Upland (Figure 2). Groundwater gathered in the upland moves down the eastern and northern slopes, draining into the Gulf of Finland and Narva River. This natural flow of water is disturbed by several fault belts and buried ancient valleys. Faults direct upper levels of groundwater to surrounding river systems. Bedrock valleys filled with Quaternary sediments intersect with deeper water layers, feeding them further. Regional hydrogeology is divided into several water complexes and layers: Quaternary, Middle Devonian, Ordovician, Ordovician-Cambrian, Cambrian-Ediacara and Proterozoic. Groundwater that tends to flow into oil shale mines originates from the first four complexes. The Quaternary complex gets its water from different kinds of sand and gravel sediments, water levels range at depths of 0.2–16 m. Middle Devonian waters come from fine-grained sandstone and reside at depths of 1–3 m. Ordovician waters gather from limestone and dolostone sectioning into three layers based on the stages they draw from. The Nabala-Rakvere aquifer, which is especially present in the Estonia and Viru mines, has its water level at 0.3–6 m, the Keila-Kukruse aquifer at 0.1–15 m, respectively. The Lasnamäe-Kunda water level can be up to 25 m deep with the depth increasing around the mining areas. The Ordovician-Cambrian water complex collects from faintly cemented fine-grained sandstones, and water levels vary. The northern areas of a mine can have water levels at 20 m and in southern areas at 160 m depth. Mining operations are greatly influenced by the hydrogeological conditions of both entire deposits and separate mining fields. To expose the useful seam of a mine the groundwater layer is breached and drained, while 10–15 m^3 of water is being pumped out per each

tonne of oil shale mined. Apart from geological conditions, groundwater levels depend on weather conditions and the mining technology used. Part of the water coming into mines is also a secondary inflow, meaning that water from drainage channels seeps back into the mine (Kattai et al., 2000).

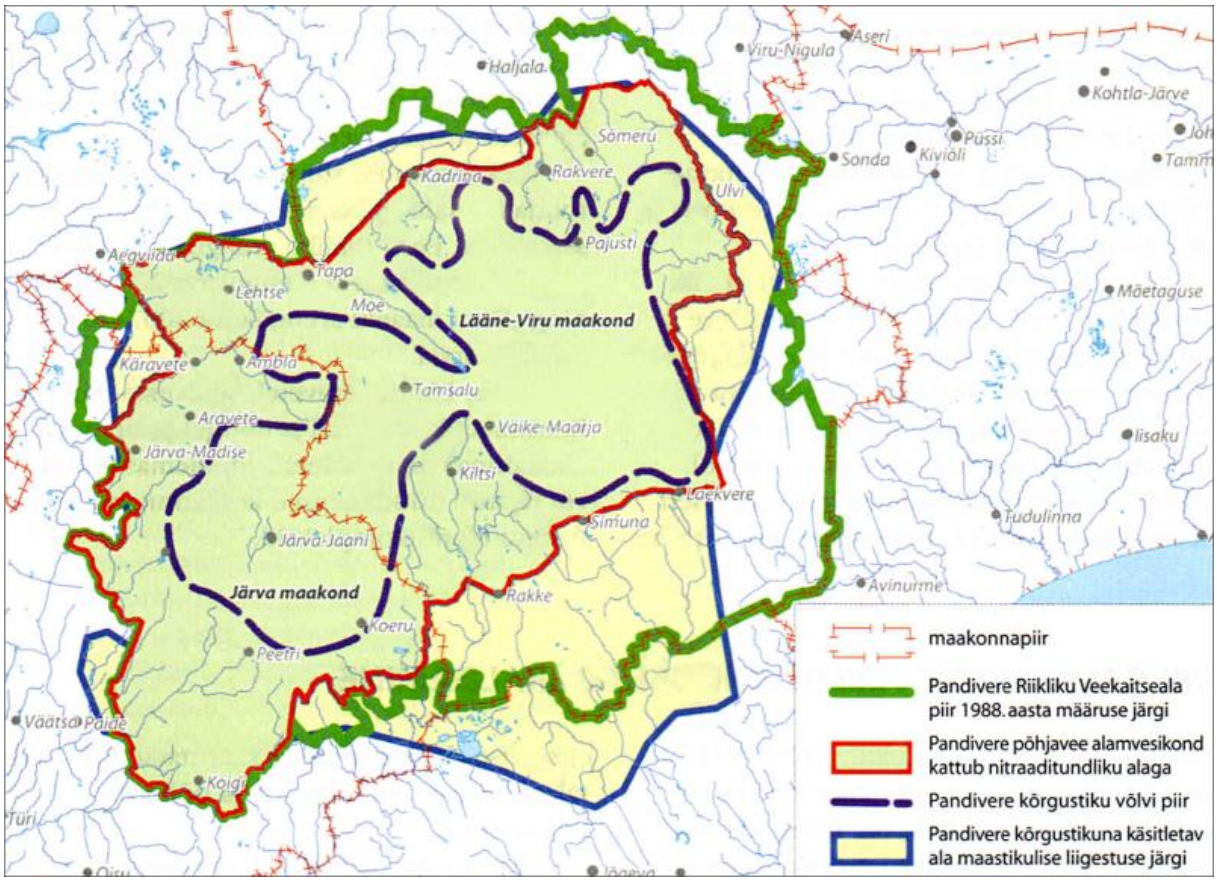

Figure 2. Pandivere Upland (Pandivere kõrgustik, n.d.).

2.3. Mining conditions

Underground mining of oil shale in Estonia takes place at depths of 10–65 m, and room-and-pillar mining is generally practised. This approach was used in the Viru mine and is currently being used in the Estonia mine. Oil shale is accessed through vertical and inclined shafts. Preparatory work includes dividing the area into panels with main entry tunnels and working faces of the panels. Most layers of oil shale are extracted while leaving pillars in place to support the roof along with anchor bolts. Mined materials are transported to processing plants. Production loss using this mining system is around 25%. Since the Sompa mine did not have a processing plant, a continuous miner was used to work on single layers, and the roof was allowed to collapse afterwards, resulting in surface subsidence. Production loss was about 26–30% (Kattai et al., 2000).

Room-and-pillar mining (Figure 3) contains a few distinct elements. Several 8-to-10-meter-long rooms are created in the oil shale blocks leaving pillars in between to support the roof. These sections are typically 300–400 m x 600–800 m in dimensions, and subsidence of the surface above the mine is minimized. Equipment used in these systems include a cutter, chain conveyer, loader, reloader, bulldozer and a belt conveyor. Haulage drifts and connecting tunnels are used to bring in fresh air and absorb blasting fumes into air drifts. Before room-and-pillar mining was taken into use, older mines such as Sompa used longitudinal section mining. One or two 100-meter rooms were dug into the oil shale blocks forming 100–200 m x 400 m spaces. Mined sections were supported by limestone pack walls or their roof was collapsed under controlled conditions when using a continuous miner. The surface above mined areas would subside 0.5–1 m on pack walls and 1–2 m on lowered sections. The rooms had pillars left between them which caused 60–100 m x 100–300 m sinkholes to form on the surface (Reinsalu, 2011).

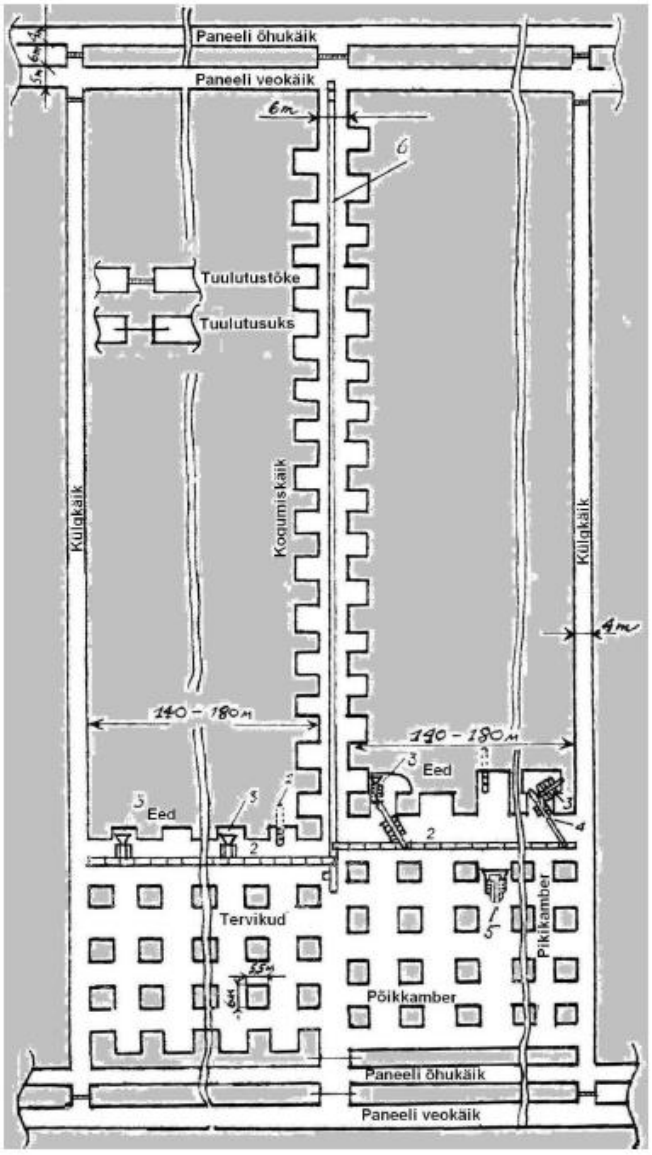

Figure 3. An outline of room-and-pillar mining (Reinsalu, 2011).

Geological conditions determine the kind of mining system, technology and equipment used, working conditions and safety measures necessary, as well as impact on the environment. Relevant characteristics of the deposits useful seam include thickness, structure and quality of the oil shale, depth, composition and thickness of overburden, geological disturbances within the rock mass and its physical-mechanical properties. Besides occasional ancient valleys and karst, the seam continues uninterrupted, which greatly benefits extraction. The mid and east section of the deposit have a seam thickness of 2.6–2.9 m with a westward gradient of 1–3 cm/km and southward gradient of 3–5 cm/km where the seam thins to a thickness of 1.8–2.2 m. The depth of the seam is an important factor, dictating the amount of preparation needed before extraction, how much is the groundwater inflow and what kind of support pillars are necessary. At the north end of the deposit kukersite is found at a depth of 1–10 m. Due to an inclination towards the south, it can reach 80–90 m at the southern border. The overburden above the useful seam can contain three different types of rock complexes which determine the overburden stability of a mined area. These complexes are loose Quaternary sediments, hard

Ordovician carbonate rocks and terrigenous Devonian sediments. An overburden thickness of 5–10 m of carbonate rocks is needed to leave a stable roof in the case of room-and-pillar mining. Physical-mechanical properties of the rock mass determine whether extraction will need to include blasting operations or if it can be done mechanically by cutting and breaking. Rock mass properties change the most around karst, porosity and moisture increase while oil shale hardness lessens and limestone strengthens due to dolomitization (Kattai et al., 2000).

The oil shale deposit is made of seven kukersite layers (A, A', B, C, D, E, F_1) and six interbedded limestone layers (A/A', A'/B, B/C, C/D, D/E, E/F_1) (see Figure 4). The kukersite layers are 5–60 cm thick and most of them contain lenticular nodules of kerogen-rich limestone. The limestone layers vary also in thickness with A'/B and C/D being 10–30 cm while A/A' and E/F_1 are 1–5 cm thick. The seam is divided into three oil shale layer complexes: A–A' is the lower, B–C the middle and E–F_1 the upper complex. This distinction is based on factors such as the differences and similarities between the layers' thickness, composition and quality of material as well as oil yield. Organic matter content can vary in kukersite between 10–65%, the richest layers being A, B and E. From a practical and economic standpoint, oil yield and productivity of the useful seam are not as relevant as the indicators between layer complexes, hence why the seam is divided into and extracted in complexes. The boundaries and thickness of individual oil shale layers within a specific complex are often rather subjectively determined. This is because some limestone layers are difficult to identify in boreholes due to their nodular texture (Kattai, 2003).

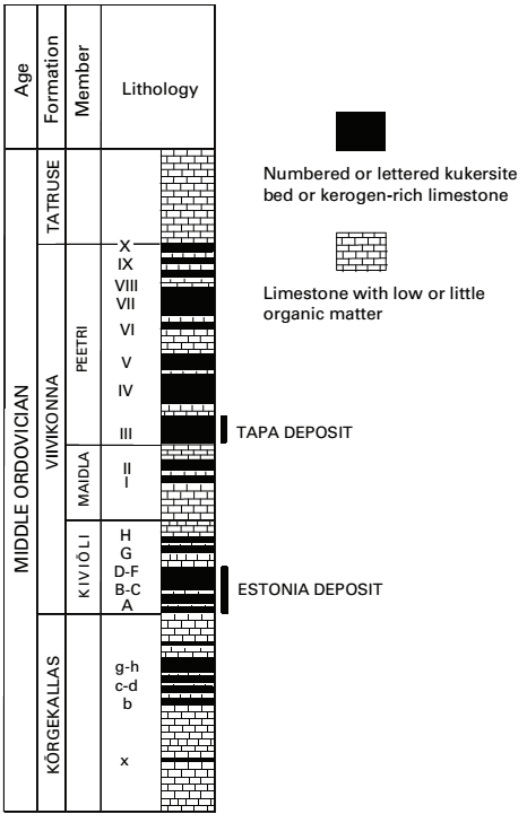

Figure 4. Kukersite and limestone layers in the oil shale deposit (Dyni, 2006).

2.4. Impact of mining

Surface and underground mining operations alter landscapes. Surface mining leaves immediate changes like pits, trenches and artificial lakes while the impact of underground operations can remain invisible for decades, especially if done deeper than 15–20 m. Active mining effects are usually predictable and manageable, but once operations cease, managing geotechnical risks becomes difficult or impossible. Mining activities are commonly followed by ground subsidence, shifting and landslides, alterations to water levels and pollution, soil heating and underground fires, gas emissions (carbon dioxide, radon, hydrogen sulfide) and overall changes to ecosystems. Collapse holes are especially dangerous in mined areas since they may reach the surface and provide access underground. In the case of oil shale mines, these holes are often found near the northern boundaries where mineral

layers are shallow, and the strength of the rock has decreased over time. Mine engineering designs typically consider safety factors to prevent structural failures, but deviations in pillar size and conditions may significantly reduce the reliability of stability predictions. For example, moisture in a flooded mine can reduce rock strength by up to 8.3 times, particularly in clay-rich rocks. Determining how long it could take for a pillar to collapse is rather difficult, depending on conditions and factors that are not always possible to be measured or evaluated accurately. A general perspective on the matter is that collapses may continue over time but not necessarily at an increasing rate, also depending on the kind of land left in the area (Reinsalu et al., 2015).

Undermined land is divided into four main categories: permanent, subsided, stable, and quasi-stable. Permanent land refers to areas where mineral resources were left unmined—either for environmental, structural, or economic reasons—and no ground subsidence occurs, except for minor shifts caused by blasting or soil drying. Subsided land forms at locations where the entire mineral layer was extracted and failure of roof support leads to visible depressions and collapse features, especially when insufficient or poorly placed fill was used. Stable land includes areas where solid support structures were left intact or mining cavities were narrow, resulting in minimal and typically completed subsidence during the mining phase. Quasi-stable land behaves initially like stable land but may undergo delayed subsidence or collapse, particularly in deeper mines or where the overburden is less than 10–12 meters thick. This type of land is considered the most problematic due to the unpredictability of future ground movements (Reinsalu et al., 2015).

To illustrate the impact of collapses towards the environment, I present photos (Figures 5 – 8) of collapses located in landscape by field expeditions.

Figure 5. Changes of landscape caused by the 2017 collapse in Estonia mine (Soosalu, 2018).

Figure 6. A hazardous area caused by the 2017 collapse (Soosalu, 2018).

Figure 7. A collapse from the year 2008 which caused the frees above it to tilt towards its centre (Soosalu, 2009).

Figure 8. A considerably large surface opening above the collapse from 2008 (Soosalu, 2009).

2.5. Study of collapse areas

Oil shale has been mined in Estonia for over 100 years since 1916, with over 130 km² having been surface mined and over 320 km² underground mined. Since the 1960s underground mining has been carried out with the room-and-pillar method, leaving behind quasi-stable ground as the load-bearing capacity of pillars decreases over time. Now, both former and current oil shale mining areas are experiencing unexpected collapse holes and subsidence depressions. These areas have been subject to numerous studies over the years and sites of previous research on collapse phenomena are often revisited. The goal is to map and measure collapses through fieldwork and analyse land use in previously mined oil shale areas. Conclusions made from these studies are multifaceted environmental impacts. Many of these impacts were caused decades ago and are appearing only now. Among dangerous collapse holes, the most hazardous ones are those caused by the caving-in of vertical mine shafts, as they can be several metres deep. Around 800 shafts are located in old mining areas that no longer have valid permits and have passed the post-mining care period. The main reason for shaft collapses is the use of wooden materials for sealing, which have long since decayed. Other impacts of ground subsidence include increased waterlogging of soil, forests dying and formation of bogs, all of which alter vegetation and hinder agriculture and forest management. On quasi-stable land, about 20% of collapses remain undetected, and 42% of subsidence areas are not visible in the landscape. These are unlikely to have a significant impact on agriculture but may damage buildings and infrastructure, reduce property values and place constraints on new construction (Vassiljev et al., 2018).

The task of seismology is to monitor vibrations in the Earth's crust caused by both natural phenomena and human activities. Through analysis of digital signals, disturbances can be identified e.g., as earthquakes, explosions and collapses. Recorded signals of each type of event are unique in the sense that they display frequency and peak amplitude changes over time. Because Estonia is a seismically a weakly active region, the most frequent seismic events recorded are explosions in quarries and open cast mines. Such activities are common during weekdays and working hours and are strictly regulated in regard with safety and environmental impact. They generate seismic events with a magnitude of up to 2. Seismic data is collected through a network of Estonian, Finnish and Latvian seismic stations. Seismograph networks are also pivotal in identifying mine collapses that would otherwise remain unnoticed. Seismographs monitor seismic activity in real-time, detecting earthquakes, explosions and collapses that generate detectable seismic waves. Seismic analysis can determine the exact time of a collapse and possibly provide an accurate enough location so that the source may be traced in the landscape. Upon finding a collapse site on land or aerial photos, seismic records may also be used in search of the time the event took place (Soosalu & Valgma, 2009).

3. Seismology

Perturbations in the Earth, such as earthquakes generate seismic waves that give information about their source and the material they pass through. To examine the mechanics of solid Earth, the principles of seismic wave propagation must be considered. Deformation of the Earth, for example during tectonic activity, causes displacements that vary over space and time. Depending on the physical properties of the Earth's interior, such as density and elastic moduli, seismic waves travel with a certain velocity and are sensitive to changes in material properties. The waves behave differently at material boundaries and interfaces, providing information about the subsurface structures they pass through. Seismic body waves are classified as primary or pressure (P) and secondary or shear(S) waves, surface waves as Rayleigh and Love waves, each having distinct propagation characteristics, as shown on Figure 9. These characteristics help to determine how seismic waves interact with heterogeneities in the Earth, which allows interpretations of geophysical data. Thus, the waves can be used to study Earth's internal structure as well as to analyse earthquakes (Stein & Wysession, 2003).

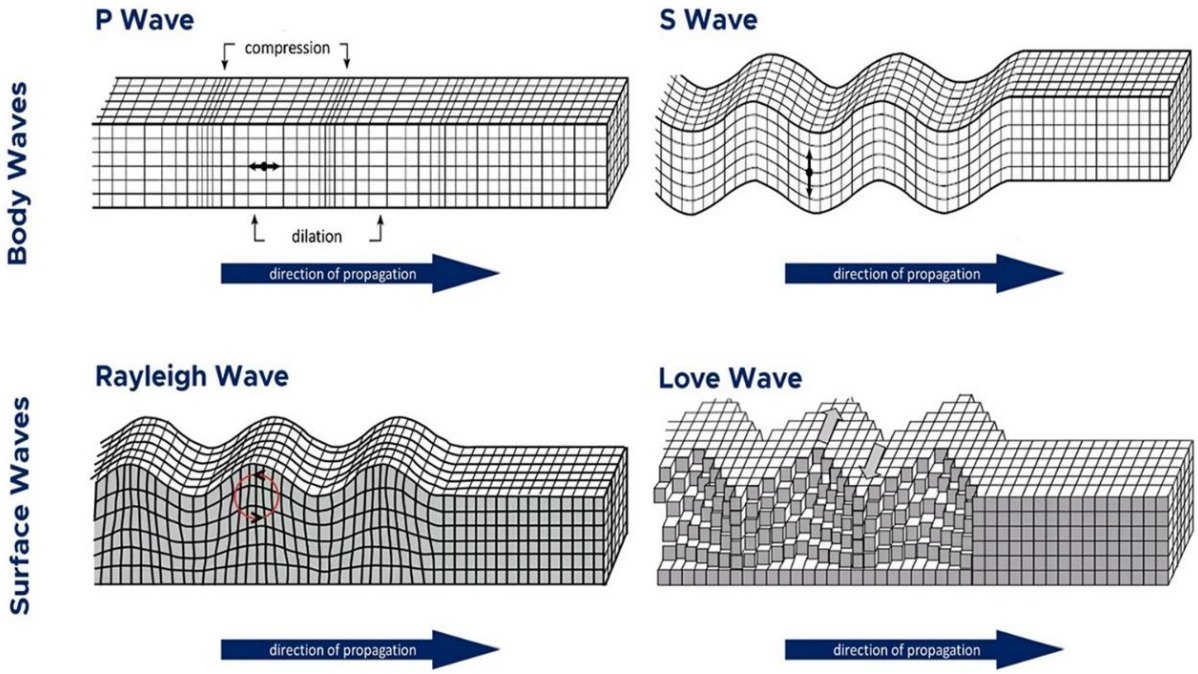

Figure 9. Propagation characteristics of seismic waves (Triton et al., 2023).

3.1. Seismicity in mining

Factors such as gravity and tectonics determine the state of stress in the Earth's crust. Mining activities disrupt the stress state in and near a mine, leading to locally increased or decreased stresses. The extent and consequences of a failure depend on three elements, geomechanical conditions, stress state and mining activity. Geomechanical conditions include intact rock with geological structures such as joints, faults and folds, also being characterized by the strength and stiffness of intact rock and joints. Failure occurs when all three factors interact and different modes of failure can occur,

depending on the characteristics of the said factors. In the event of high stress levels, rock mass that contains low strength rock types and has a low quality may display massive failures and plastic deformations. Rock mass that is of high quality and consists of brittle high strength rock types may have an even higher risk of violent failure. Increasing mining depth in underground mines leads to higher stress levels and a heightened risk of instability in drifts, ramps, shafts and other structures. Other phenomena such as activation of faults may also become more frequent at greater depths and a fault slip is capable of releasing large amounts of destructive energy. Violent failures may hinder production, damage equipment, collapse tunnels and pose a safety risk to mine personnel, especially people close to the working face. These types of failures are generally called rockbursts. Seismicity is the rock mass response to deformation and failure, while a seismic event is the sudden release of potential energy in the rock which radiates as seismic waves. Therefore, a rockburst is defined as a mining-induced seismic event that damages openings in rock (Larsson, 2004).

Collapse events are a serious concern in mining operations and can be divided into three types of rock failure processes in underground environments. Progressive failure begins with localized fractures triggering further failures in adjacent layers, continuing until the system restores balance or a roof fall occurs. This is common in room-and-pillar mining environments. Episodic failure is characterized by periods of apparent stability followed by sudden large-scale collapses often triggered when stress in a large unsupported area exceeds structural capacity. Longwall mining with strong roof strata and limited panel sizes is especially susceptible to such failures. Continuous failure is also associated with longwall mining, characterized by wide panels, a heavy overburden and limited adjacent support. As mining advances, rock failure is regular and predictable, often in sync with the mining pace. The nature of roof failures is influenced by several conditions. The composition of the roof strata—including the layering, strength, and stiffness of the rocks—affects how failure initiates and progresses. Horizontal and vertical stress conditions determine whether failure occurs through buckling, shearing, or tension. Mining geometry, such as panel width, overburden depth, and excavation method impact the failure behaviour. Additionally, support conditions provided by adjacent or underlying strata influence the overall stability of the roof. Roof failure typically begins with the buckling of stiff, thin layers under high horizontal stress, followed by the propagation of shear and tensile fractures. As structural support weakens, fractures can lead to the collapse of roof beams, often resulting in an arch-shaped cavity. This collapse redistributes stresses, which may trigger further failure at the edges of the affected area (Iannacchione et al., 2005).

3.2. Destructive forces of a collapse

An underground rock mass collapse is a combination of several hazardous aspects. A collapse may consist of factors such as the sudden movement of large amounts of material in an enclosed space, openings forming close to or on the surface, damage to equipment and structures both underground and above and a threat to anyone in the vicinity. In addition to this, water and air may also become quite hazardous. Water must always be considered in the planning of mining activities to avoid flooding and contamination of groundwater. After a mine is closed however, cavities may still flood which in turn, as mentioned in section 2.4., increases the likelihood of collapses occurring. A collapse in a

flooded mine can cause a potentially dangerous water outburst. As an example, if there are flooded tunnels at a depth of 40 m, the water level may not be high enough to provide support for the walls and roof. A collapse with an area of 2500 m^2 lasting one second would transfer an impulse of 2.5×10^6 kg·m/s, or 2.5 MN·s, to the water, thus creating a pressure wave. If the wave does not have enough space to attenuate within the mine, it will seek weaker exit points such as cable ducts, boreholes, shafts leading to the surface and tunnels connecting to other mines. Once the wave finds an outlet, especially in the form of small openings, the speed of the pressurized water can become extremely high, ejecting tens of tons of material from sealed boreholes and shafts as well as conduit sleeves of cable ducts (Reinsalu et al., 2015).

Like water, air also has the potential to cause severe damage. Underground cavities act like air chambers and when a roof collapses, suddenly decreasing the volume of these voids, the air is compressed and forced to escape at high speed through available tunnels and shafts. Also known as an air shock, this rapid compression and expulsion of air is driven by differences in pressure, its intensity depending on the extent of the collapse. In extreme cases, such as the 2005 Xingtai gypsum mine collapse in China, an air shock can reach a velocity of over 600 m/s, nearly twice the speed of sound. The shockwave travels through tunnels with a devastating force, rebounding and reversing direction upon hitting obstructions. Such incidents pose a serious threat to miners, equipment and mining structures (Wang et al., 2008).

4. Analysis of seismological data

Seismology determines the seismic velocity distribution within the Earth, which influences its elastic, mineralogical, chemical, and thermal properties. This distribution defines the Earth's internal structure, offering critical information that other geophysical methods (e.g., gravity, magnetism) cannot resolve as precisely. Primary data in seismology are travel times of seismic waves between a source and a receiver. These travel times reflect the integral of slowness (1/velocity) along the ray path. Because waves bend or refract through varying velocity media, the observed travel time provides an integral constraint, not a unique path or velocity distribution. Solving this inverse problem—deriving velocity structure from observed travel times—is a challenge, as many velocity models can satisfy the same travel time. While wave velocities primarily vary with depth, the Earth also exhibits lateral heterogeneity—variations in velocity at the same depth—indicating complex structural and compositional differences. Ultimately, seismological theory allows us to model how waves interact with Earth's internal layers and provides the mathematical and physical framework to extract structural information from seismic observations (Stein & Wysession, 2003).

When processing seismic data, the event type is determined along with an estimate of its distance. The primary task in analysis is to pick arrival times of seismic phases (P and S wave), which allow event location. The P and S wave arrivals should be clearly distinguishable on a seismogram, with S often having the largest amplitude. However, noise, scattered waves and multiple phase arrivals can make seismograms more complex. Digital filters are used to help differentiate between phases and pick their arrival times, but too much or incorrect filtering may cause phase shifts. Utilizing data from multiple seismic stations in close proximity of each other may serve to enhance signal detection by improving the signal-to-noise ratio. Estimations of wave direction and speed through time-delay analysis can also be made with several stations (Ottemöller & Havskov, 2010).

4.1. Noise and filters

Seismometers must have sensors sensitive enough to record small seismic signals, but this means earth noise will also be present in the recordings, creating a parameter known as signal-to-noise ratio. Noise is caused by many factors, such as solar and lunar tides within solid earth, fluctuations in temperature and atmospheric pressure, storms, human activities and ocean waves. Most noise is in the frequency range of 0.1–0.2 Hz. To lessen the surface noise input, seismometers are often installed, for permanent use, in boreholes or, for temporary use, less than a metre beneath the surface, thus avoiding noise, for example from rain and wind, which generate high frequency and long-period noise (Stein & Wysession, 2003).

Filtration enhances specific features of a seismic signal while suppressing others. There are three types of filters used in signal processing. A high-pass filter at frequency f_1 removes low-frequency components and a low-pass filter at frequency f_2 removes high-frequency components. Bandpass filters remove both high- and low-frequencies outside a specified range. These filters are defined by corner frequencies (f_1 and f_2), where the amplitude decreases to 0.7 relative to the unfiltered signal (Ottemöller & Havskov, 2010).

4.2. Signal stacking

Stacking is a technique that combines multiple seismic measurements to enhance a desired signal and reduce random noise. Stacking can be done by averaging measurements such as arrival times from different seismic records or by summing full waveforms from multiple seismograms before extracting parameters. This helps to improve precision, filtering out irrelevant or misleading features. When adding seismograms at nearby stations, the assumption is made that they contain a common signal of interest and noise that differs between stations. The noise consists of differences in the response of the seismometers and in the seismograms generated by interactions between the seismic waves and crustal structure under each station. If the seismometers and crustal structure are similar enough, stacking should reduce noise and yield a clearer representation of the signal (Stein & Wysession, 2003).

4.3. Comparison of seismic events

Modern seismometers are advanced instruments capable of detecting a wide range of ground motions, from slow, long-period signals associated with Earth tides to rapid, high-frequency vibrations generated by nearby earthquakes. Because no single sensor can effectively capture the full range of seismic activity, different instruments are used to target specific frequency and amplitude ranges. Broadband digital seismometers utilize force-feedback technology to maintain high sensitivity and a flat response over a wide frequency spectrum. This allows them to accurately record both large and small seismic events. Modern systems also incorporate precise timing using GPS signals, ensuring accurate synchronization of seismic data across global networks and improving the reliability of earthquake analysis and early warning systems (Stein & Wysession, 2003).

Signals recorded by seismic tools present the arrival times and peak amplitudes of P, S and surface waves, which are visualised with seismograms and spectrograms. Spectrograms are especially helpful in differentiating between seismic events of varying origins. Below is a visual comparison of an earthquake, a quarry explosion and a mine collapse (Figures 10–15). I created the figures using the ObsPy library, a Python framework for processing seismological data (ObsPy, i.a). The scripts read seismic data from a file containing the signal of an event through three channels, vertical (Z) and horizontal north-south (N) and west-east (E). I then applied a high-pass filter of 0.8 Hz to remove low-frequency noise, resulting in a seismogram that showcases the event more clearly. The spectrograms are plotted for the Z-component of the seismic signal as the time-frequency representations of said signal. All signals are recorded in UTC time and the locations of seismic stations are shown in Figure 16. An example of a seismic data visualization script in Python is shown in Appendix 1.

4.3.1. Earthquake

The first event is an earthquake that took place in Väike-Maarja, Lääne-Viru County, on the 14th of March 2020. It had the magnitude 1.3 and its epicentre was determined as 59.132°N, 26.254°E (Soosalu, 2021). Below are the 0.8 Hz high-pass filtered seismogram (Figure 10) and spectrogram (Figure 11) of the event detected by the Finnish seismic station VJF at the distance of 173 km. The

seismogram shows 3-component recordings of the signal, i.e., Z, N and E. I have highlighted the P-wave arrival time on the Z-component and S-wave on the E-component. Although the recording contains also noise, the signal is still visible enough to discern two amplitude peaks in the seismogram, typically observed in earthquake detection. P-wave is always the first to arrive followed by S-wave, being about 20 seconds apart in this case.

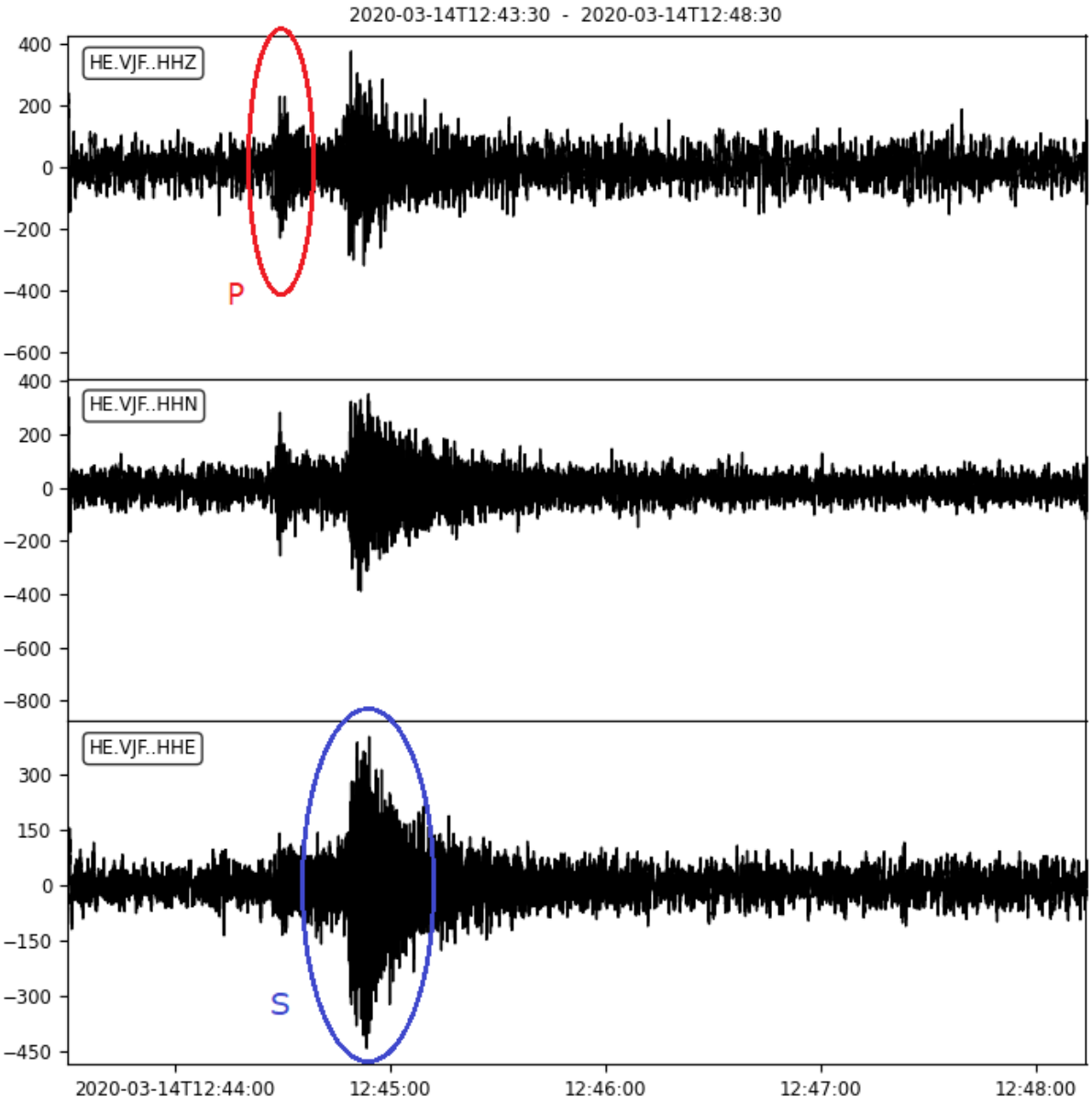

Figure 10. Z-, N- and E-component seismograms of the station VJF for the Väike-Maarja earthquake.

A spectrogram of the earthquake visualizes the signal even more clearly. Bright colours indicate the presence of signals caused by noise and seismic events. Background noise is constant around 1 Hz and at 60 seconds is when the signal arrives, creating two higher frequency traces with a range of 0.8–20 Hz at P- and S-wave arrival. The traces colours are also even throughout the frequency range, meaning that no single frequencies are dominating.

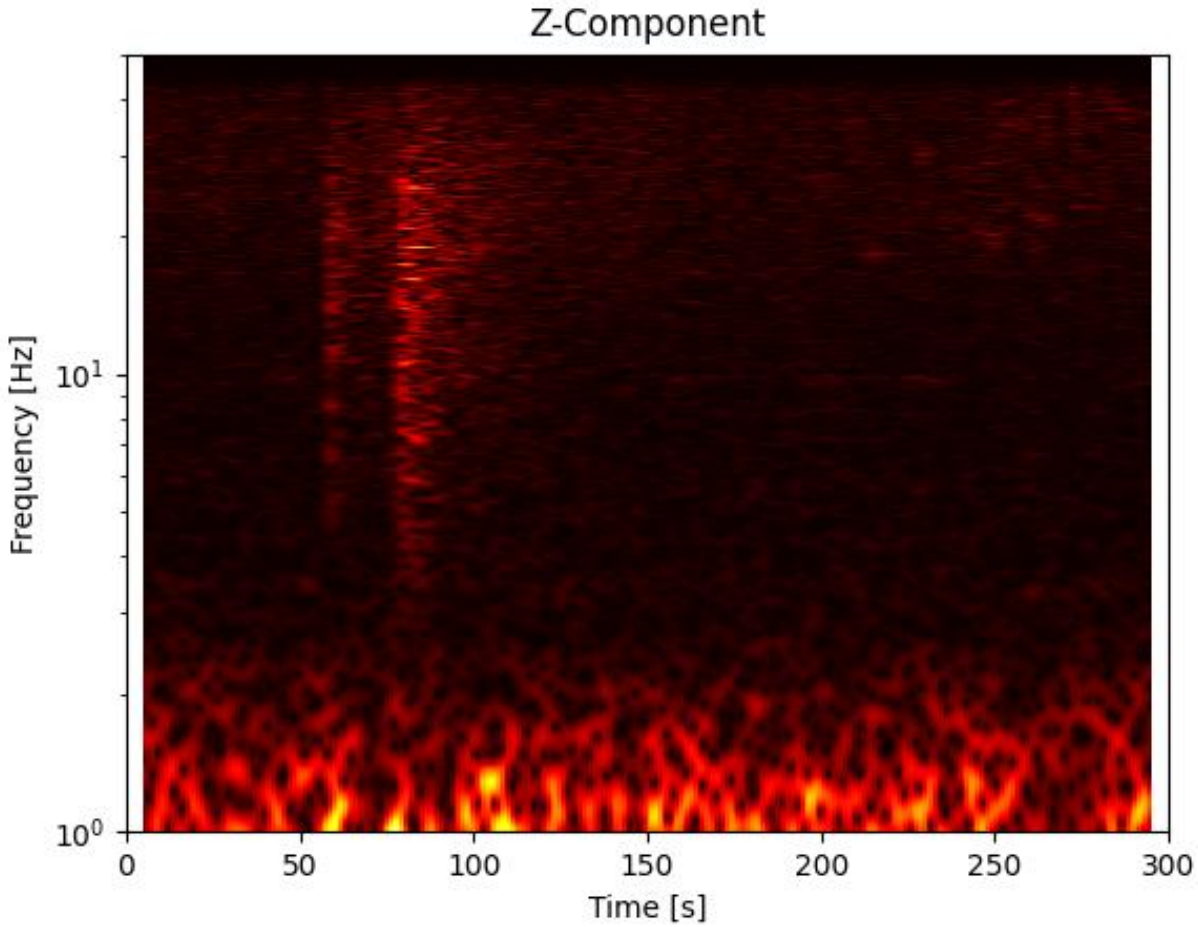

Figure 11. Z-component spectrogram of the Väike-Maarja earthquake.

4.3.2. Explosion at an open cast mine

The figures 12 and 13 show an explosion at the Narva open cast mine on the 1st of November 2023. The magnitude of this event was 1.8 and its epicentre located at 59.219°N, 27.900°E (Soosalu, 2024). I used the recordings of the PISE station located in the Piusa caves 156 km away. This station provided a rather clear signal of the explosion with little noise interference. P- and S-wave arrivals are clearly visible, arriving 20 seconds apart, but the explosion signal appears to attenuate away less gradually than the signal of the compared earthquake.

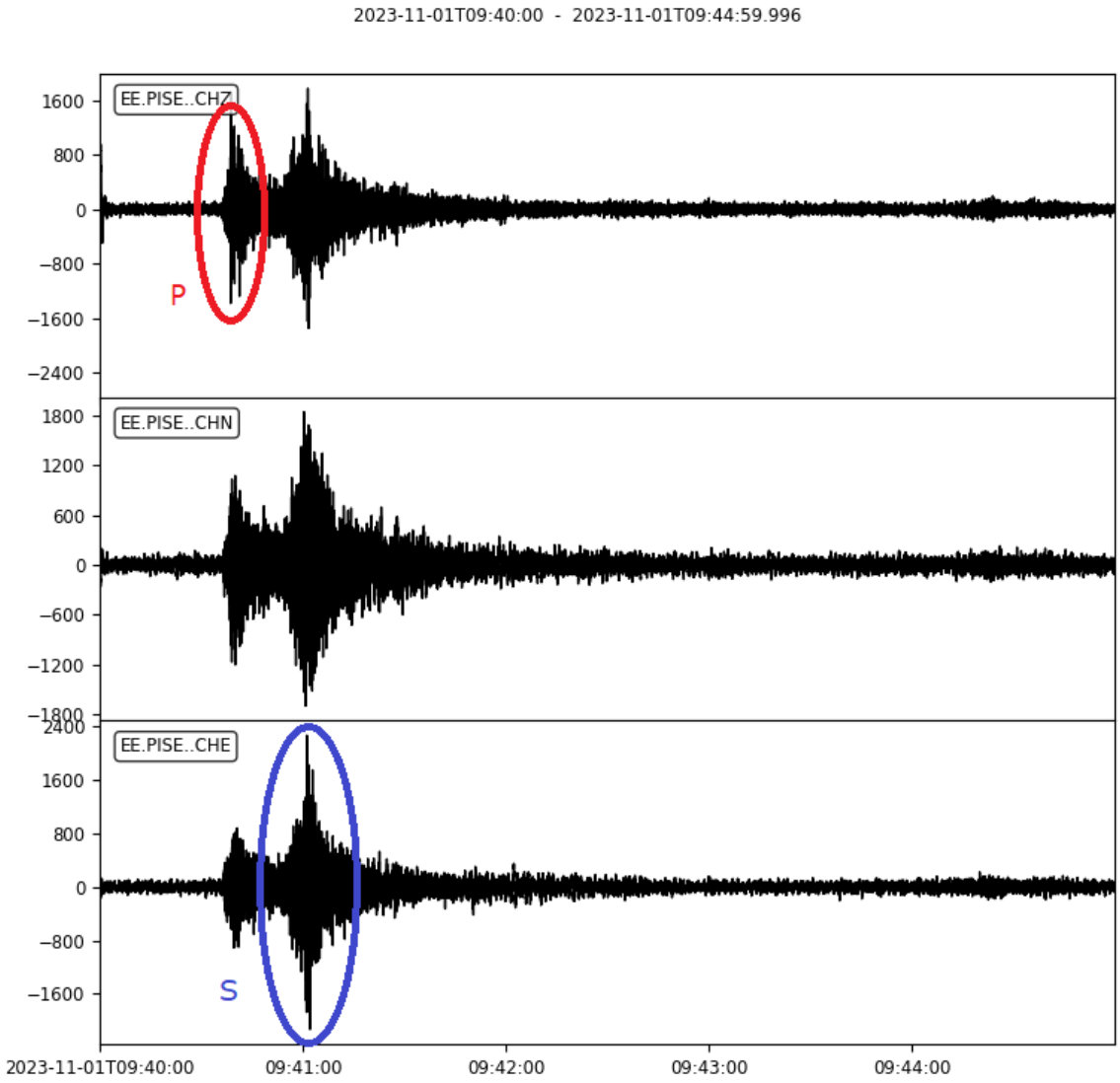

Figure 12. Three-component seismograms of the Narva open cast mine explosion at the station PISE.

Comparing the explosions spectrogram with the earthquake signal highlights the broader frequency range of the earthquake, while the range of the explosion is much smaller. The typical “stripey” appearance of an explosion spectrogram, due to a few dominant frequencies, can be vaguely seen in this case.

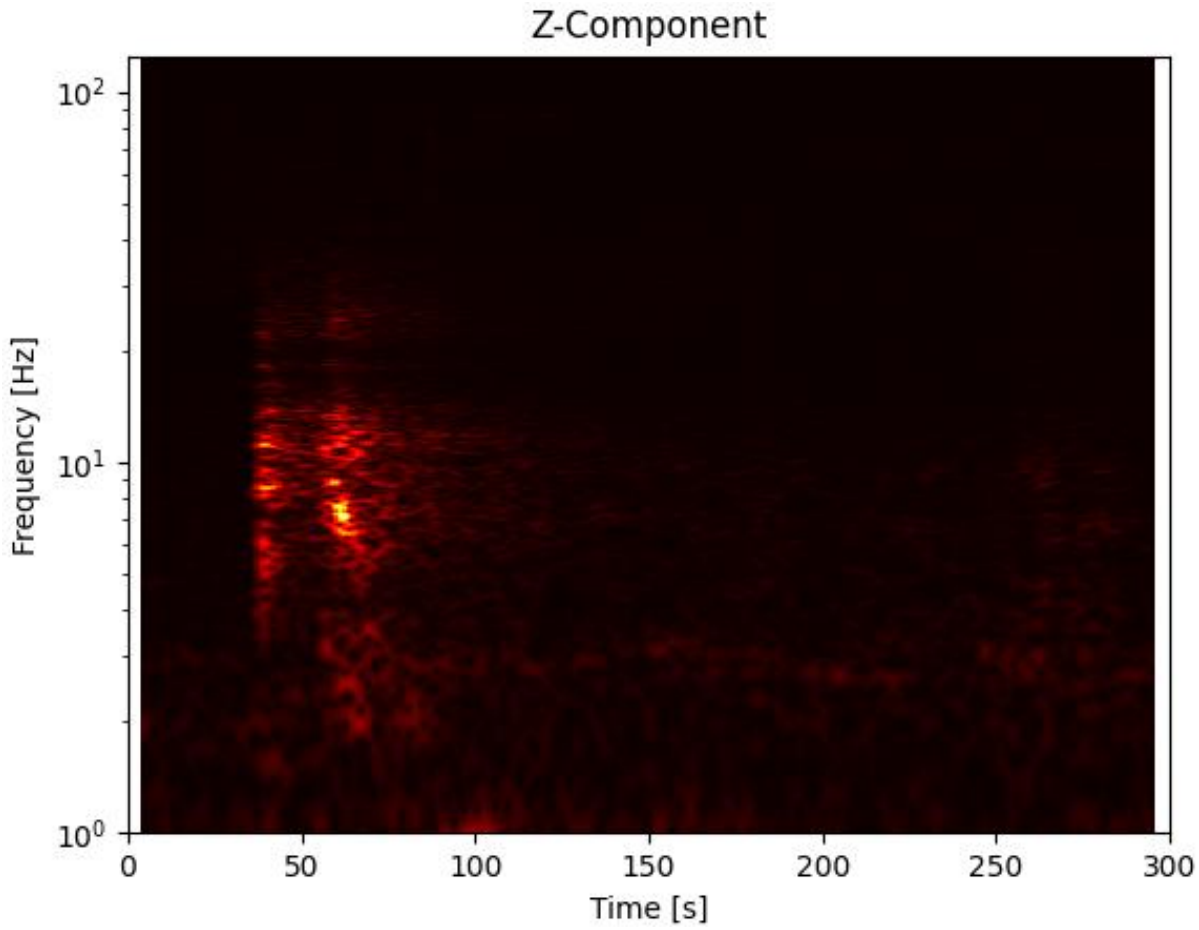

Figure 13. Spectrogram of the Z-component recording of the explosion.

4.3.3. Mine collapse

Last, I have analysed a collapse in the Estonia mine on December 24th, 2023, with the epicentre at 59.207°N, 27.415°E (Soosalu, 2024). The station PISE provided a relatively noise-free signal recording for this event, as well (Figures 14 and 15). The magnitude of this event was 1.6. P- and S-wave arrivals are 18 seconds apart. But the signal that follows is, among these three types of seismic events, unique only to the collapse. This event has a much longer duration, lasting several minutes with what seems like more than two peak amplitudes, highlighted with a green line on the figures.

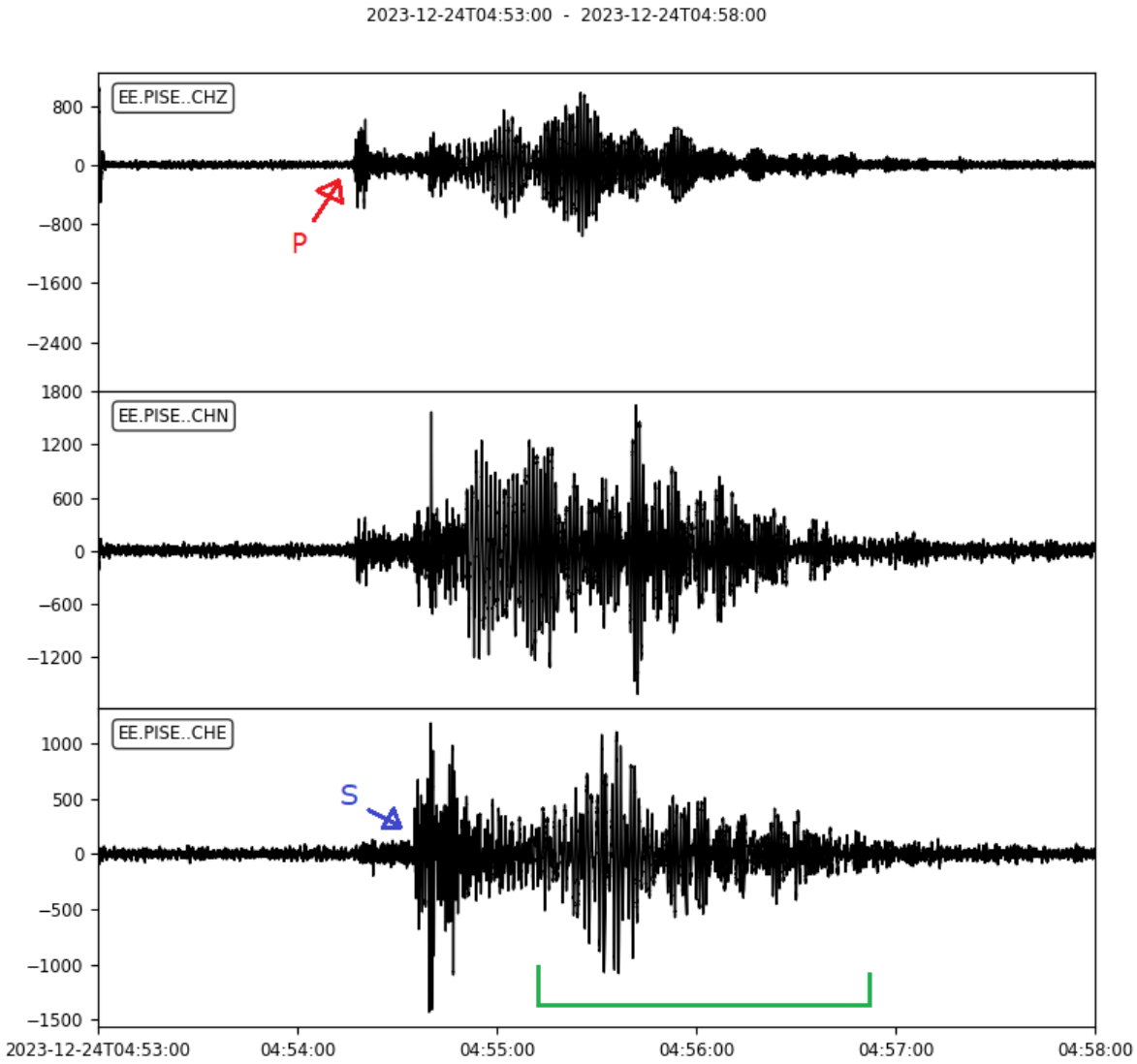

Figure 14. Seismograms of the collapse that are strikingly different from the previous events.

A spectrogram of the collapse event also shows a difference in frequency range compared to the previous events. The seismic waves generated by the collapse are at a much lower frequencies, around 1 Hz with the arrival time peaks being short pulses similar to an explosion. The arrival times are followed by another lower frequency wave that lasts for nearly two minutes. The cause of such a long signal could be that when a roof collapses in an underground mine, the generated seismic waves travel through the expanse of the mined-out tunnels, reflecting and redirecting off the cavity walls, thus prolonging and enhancing the original signal. This could be similar to how soundwaves reflect and resonate within the cavity of a musical instrument, with some frequencies being reinforced and some dampened.

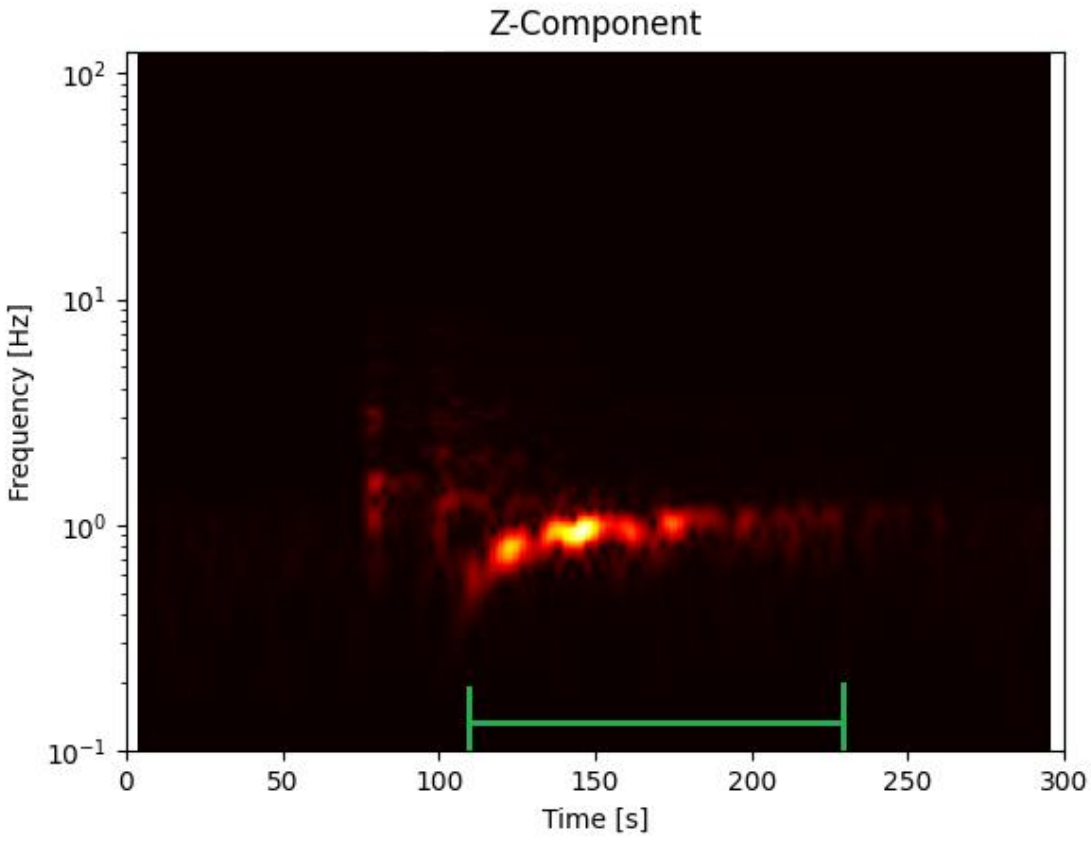

Figure 15. Z-component spectrogram of the collapse, presenting the unique low-frequency "tail".

5. Methodology

5.1. Event isolation and seismogram clipping

Before analysing seismic data, I familiarized myself with the Finnish and Estonian station network and viewed a few examples of data registered by these seismic stations (Appendix 2). I compared seismograms of quarry/open cast mine explosions, earthquakes and mine collapses and, based on earlier records, I determined P and S wave arrival times on the seismograms. The next task was to find which seismic stations had the clearest recordings of collapses from the Estonia, Sompa and Viru mines. I considered all Estonian stations and several Finnish stations that were close enough or had especially clear signals. I used different high and low frequency filters to see which stations had the most visible event signals. I then selected 16 Estonian and 18 Finnish stations (Figure 16), the closest station from the Estonia mine being EE04 located some 30–35 km away and the furthest JOF at over 460 km distance. I included JOF, because it has provided relatively clear recordings of Estonian seismic events, despite the great distance. This station is also important due to its location from the Estonia mine, being the only available station that has a more eastern longitude than the mine. Locating a source of a signal gives more precise results when there are stations in every direction of the source, thus decreasing the margin of error. Systematic location errors may occur if there are observing stations only in a narrow sector.

Next, I needed to isolate the collapses and clip 5-minute sections from the recordings with the beginning of each clip starting half a minute to one minute before the arrival time of the signal. A strip of preceding seismogram before the onset of the signal is needed for identifying the level of background noise. I used a shell script to clip each event in preparation for further analysis. With these selected clips, I tested data from different seismic stations to compare seismic events (described in the previous chapter) and to analyse collapses through different perspectives, which will be introduced in following chapters. Below is Table 2 which shows the locations of all seismic stations used for analysis.

Table 2. Locations of all stations used for analysis. Other stations were used for testing but not for conclusions. Coordinates from Soosalu, 2025 and Institute of Seismology, 1980.

Station	Latitude	Longitude	Altitude (m)
ARBE	59.43650	25.98410	71
EE03	58.87280	26.27280	89
EE05	59.39150	27.91980	26
EE06	58.96950	22.84820	6
PISE	57.84140	27.46740	75
VJF	60.5388	27.5550	34
VSU	58.46200	26.73469	63

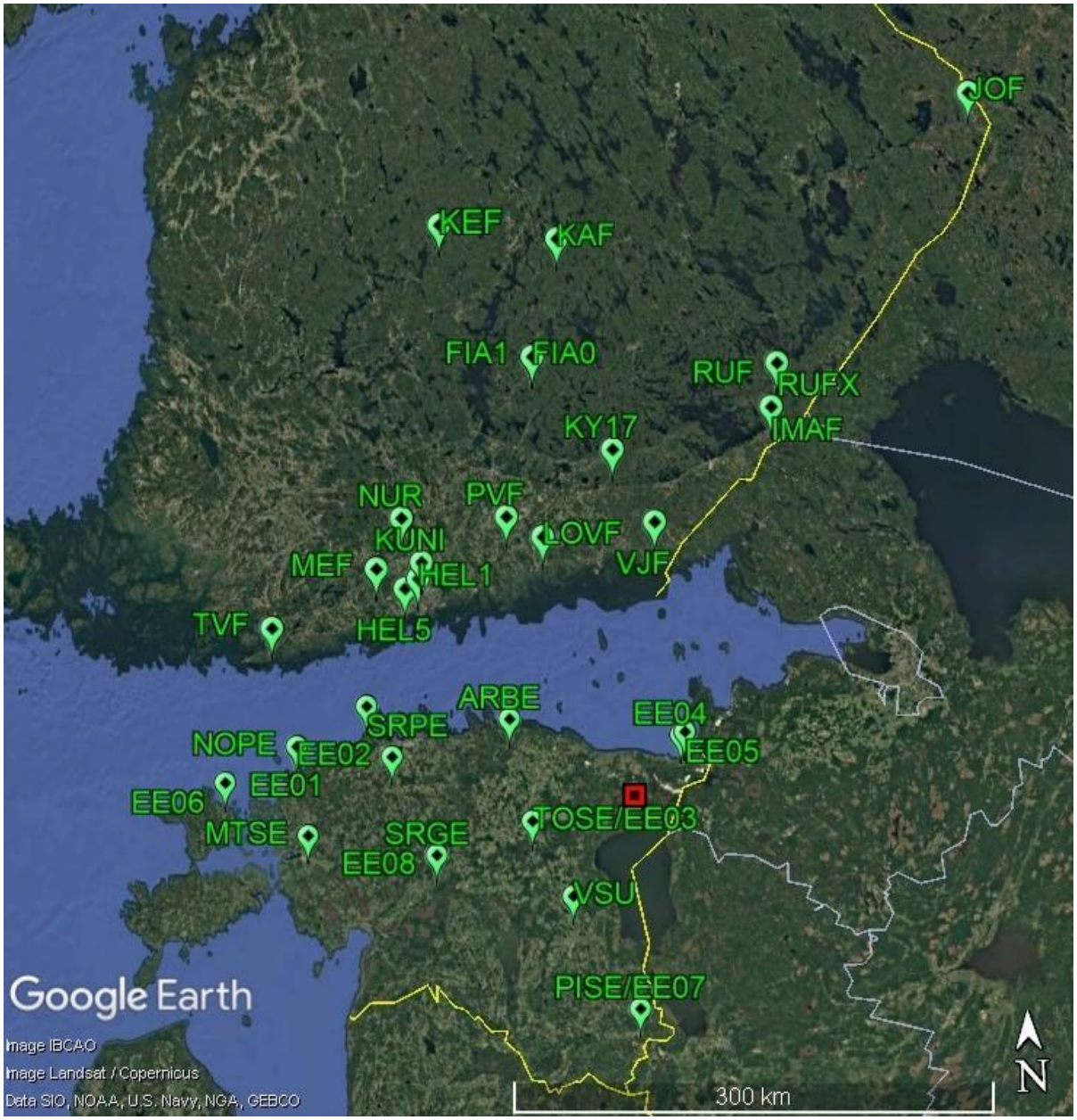

Figure 16. A map of all seismic stations used or considered for data analysis.

The red marker shows the approximate location of the oil shale mines.

5.2. Signal filtration

With the data sorted and clipped, the next step was signal processing. The data I now had was unfiltered, which makes picking P and S wave arrival times more difficult. By processing the signals with filters of 0.8–20 Hz, I was able to eliminate most of the noise on the seismograms, thus leaving a

clearer signal from an event. Figure 17 shows an unfiltered seismogram as it is, with noise and seismic event arrival times being near impossible to discern from one another.

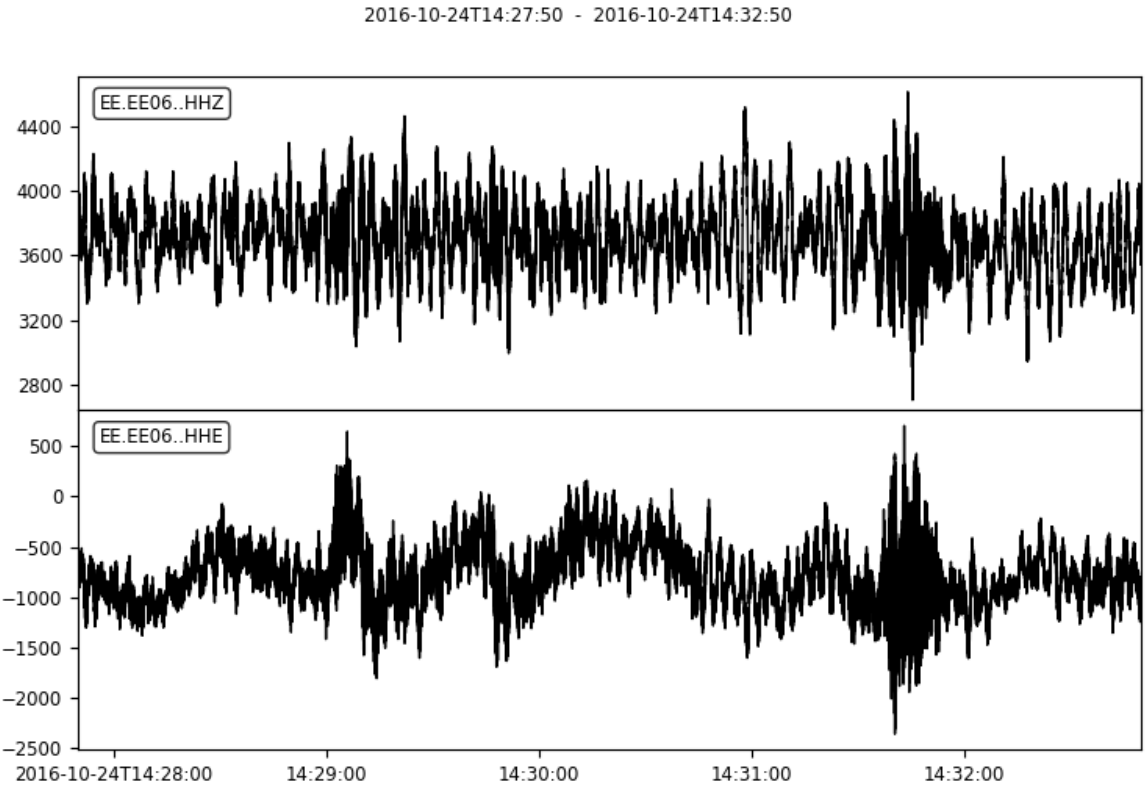

Figure 17. Unfiltered seismograms of the Z- and E-components of the station EE06.

5.3. Stacking

Collapses during the year 2016 were interesting in the sense that there were four events, two of which took place on the same day, March 4th hours apart (01:23 and 22:45 UTC, magnitudes 1.5 and 0.9). Two collapses seemingly occurred very close to each other, but months apart – the smaller March 4th event and another one with magnitude 1.5 on October 24th. The issue is that it seems more logical that two collapses taking place on a same day are expressions of the same process in an approximately similar location rather than two events take place near each other with delay of several months. The signal-to-noise ratio of the magnitude-0.9 event was poorer than the two other magnitude-1.5 events. Accordingly, its seismic location may be considered less reliable.

I used data from these three events, recorded at the station EE03, to test the signal stacking technique, introduced in chapter 4.2. Stacking two signal pairs – the two March events and the weaker March event with the October event may enhance ability to draw conclusions regarding the location of the smaller collapse in March.

I used a Python script to stack the signals lined up according to the P-wave arrival times. This script used 1,5–2-minute-long seismogram clips from the station EE03. It created trace files starting from 5

seconds before the arrival of P-wave and ending 11 seconds later, with S-wave arriving 2 seconds before the cut-off. I chose this section of data so that the distinction between noise and data would be visible along with the seismic wave arrival times. I entered the original binary data in plain ascii numbers into Excel. In Excel, I summarized the data for each component (Z of the first event + Zof the second event, etc.) and created charts (Figure 18) comparing the Z, N and E component data with summarized values. Comparing both collapses in March showed considerable overlap between the signals, suggesting that the two collapses may have occurred closer to each other than initially thought. Comparing the smaller collapse with the October event also showed a certain amount of overlap, but the result was not as clear. Signal stacking is typically done using data from multiple stations, which would also be necessary in this case to provide a more detailed analysis. A larger dataset may allow the epicentre of a collapse to be more precisely located, providing more definitive evidence on the true location of the weaker collapse. Such a small collapse may be more difficult to find in the landscape, which poses safety risks. By using seismological data to help pinpoint locations of collapses, it can be ensured that openings in the ground are found and dealt with according to safety regulations.

The charts in Figure 18 show signals of individual event signals with an orange line and stacked signals with a green line. The red and blue vertical lines mark the arrivals of P- and S-waves of the events that are compared with the stacks. Chart A) compares the magnitude-1.5 collapse in March with the stacked seismogram of both March events. Chart B) shows the magnitude-0.9 collapse with the stacked March events. C) compares the magnitude-0.9 collapse in March with the stacked seismogram of the 0.9 and the October magnitude-1.5 events. D) shows the October magnitude-1.5 collapse with the stacked values of the March 0.9 and October 1.5 events. Seismogram amplitudes are in arbitrary units.

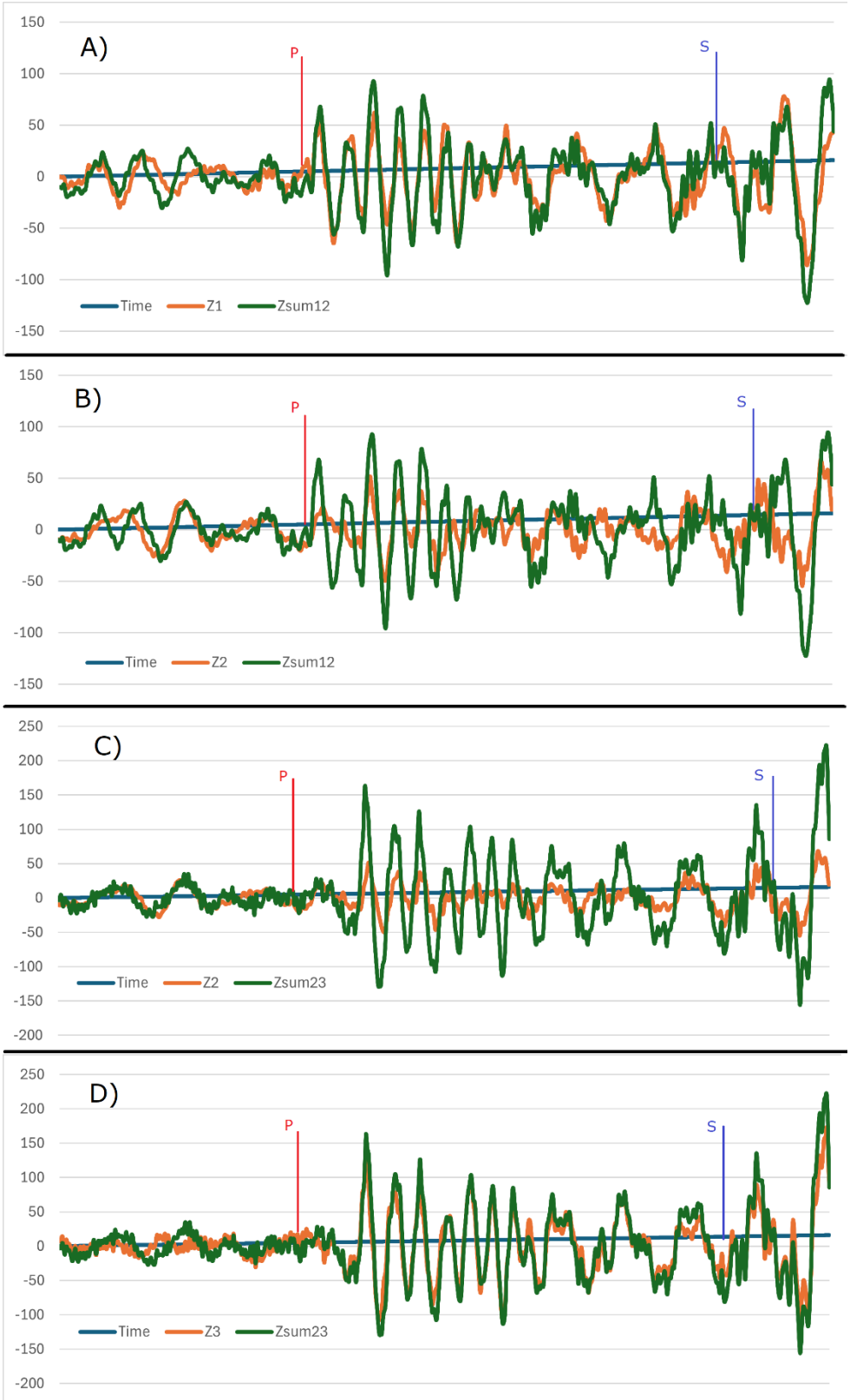

Figure 18. Comparisons between seismograms of individual events and two-event stacked seismograms.

6. Results

The aim of this thesis was to find possible patterns or correlating causes for times and locations that collapses took place in the mines Estonia, Viru and Sompa. I considered factors such as the date, separately looking at the distribution by months, days and times, location in relation to geological features such as known faults and karst zones and possible meteorological conditions, such as season and weather conditions. An additional factor is that two of the three mines are inactive. Below I present multiple charts that view the events from the perspective of separate factors.

It is worth noting that the Estonian and Finnish network of seismic stations that provided data for this thesis have been expanded during the study period and some existing stations have had their equipment updated. In particular, the number and distribution of stations in the Estonian network has been improved considerably from 2015 on. It is reasonable to assume that it is unlikely for any collapse events with a magnitude greater than 1.5 (possibly even from a magnitude of 1) to have gone undetected by the combined network.

6.1. Time related factors

Figure 19 shows a cumulative chart of the collapses over a 16-year period. The collapses have been occurring periodically, 2015–2017 being the most active time, and collapse-free periods became shorter after every event period. In 2016 there was one collapse in the Sompa mine and three in the adjacent Viru mine. The events in both mines took place months apart and within a little over five km radius of each other. These inactive mines had been stable for at least eight years before the collapses (based on the seismic data used for this thesis) and have been stable since. The Estonia mine has had seven collapses, two in 2008, two in 2015 and the rest at intervals of two to three years. Based on this overview, the collapses at Sompa and Viru seem more as single-event occurrences, while Estonia is experiencing periodic collapses, possibly at an increasing rate.

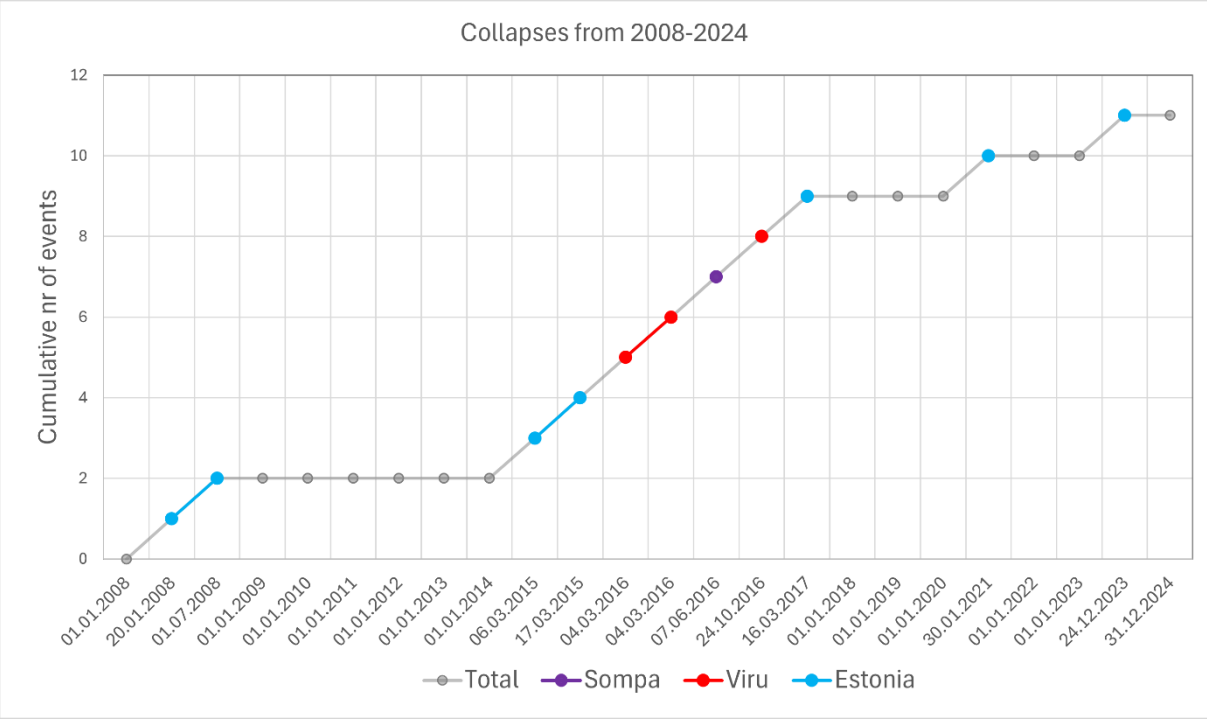

Figure 19. The 11 collapses over a 16-year period.

The next four charts, Figures 20–23, focus on collapse distribution by months, days of the week and both UTC and local times, respectively. Collapses have occurred in the months of January, March, June, July, October and December, with most events taking place in winter months and March. This distribution is most likely related to seasonal conditions, which will be discussed further in paragraph 6.2. The weekday distribution revealed collapses are more frequent at the beginning and end of the week, with most collapses occurring on Tuesdays, Fridays and Sundays. The time distribution showed that while few collapses happened during the day, most of them were concentrated around night and early morning. In the case of the Estonia mine, this would suggest a correlation with the mines working hours, specifically when workers' shifts begin and end. One can speculate if switching off the ventilation systems for the night and a change in airflow may affect air pressure and trigger a collapse that was more or less ready to occur any time. An increase in humidity during the night-time may also contribute to the weakening of mine structures. It is possible that a combination of such subtle changes in the mine environment may be enough to increase the likelihood of a collapse.

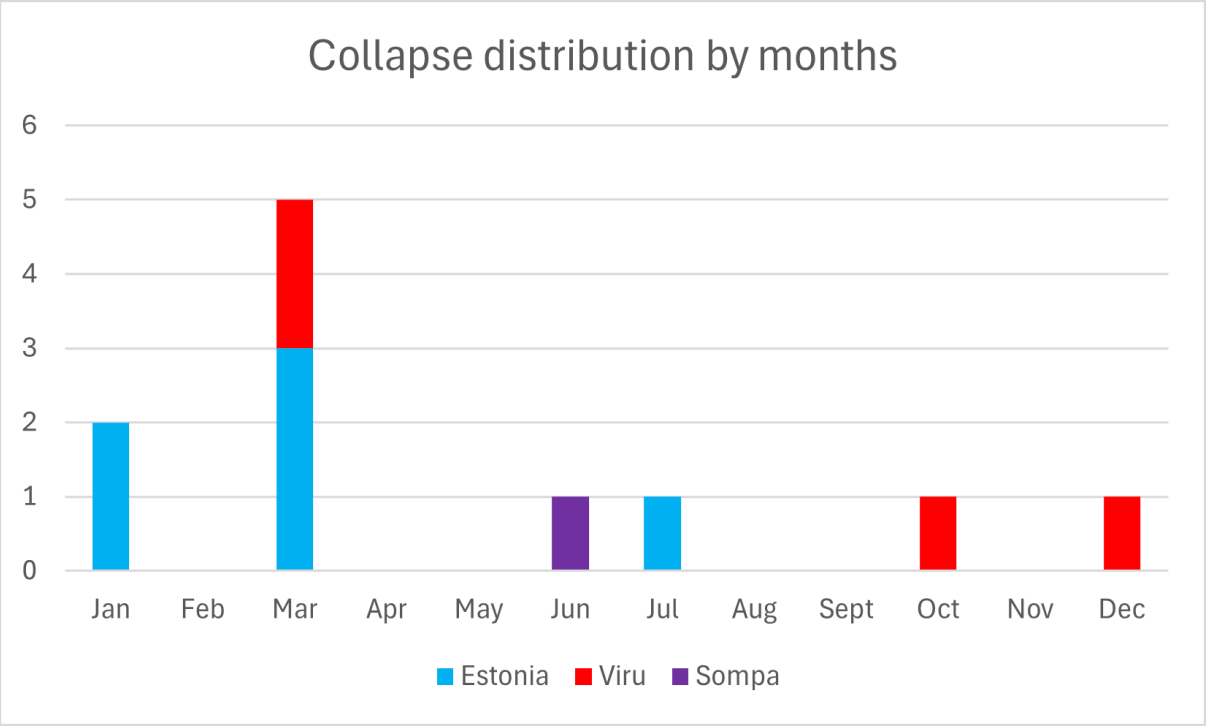

Figure 20. Distribution of collapses by months.

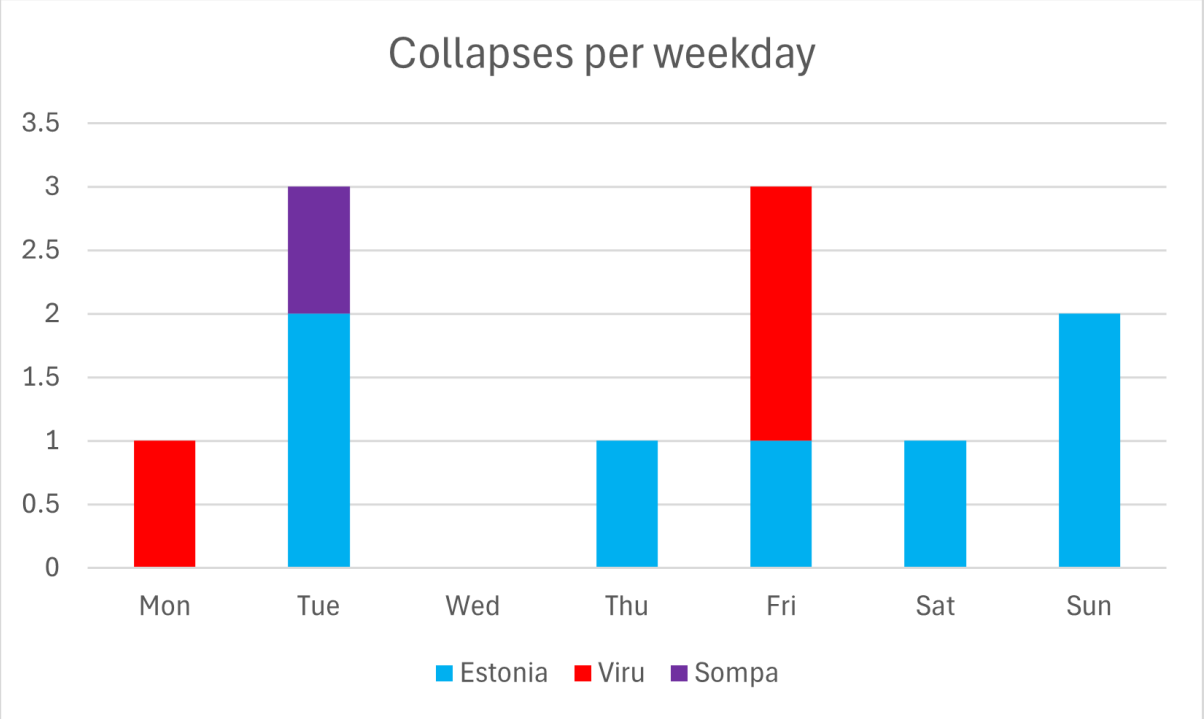

Figure 21. The distribution of weekdays when collapses have occurred.

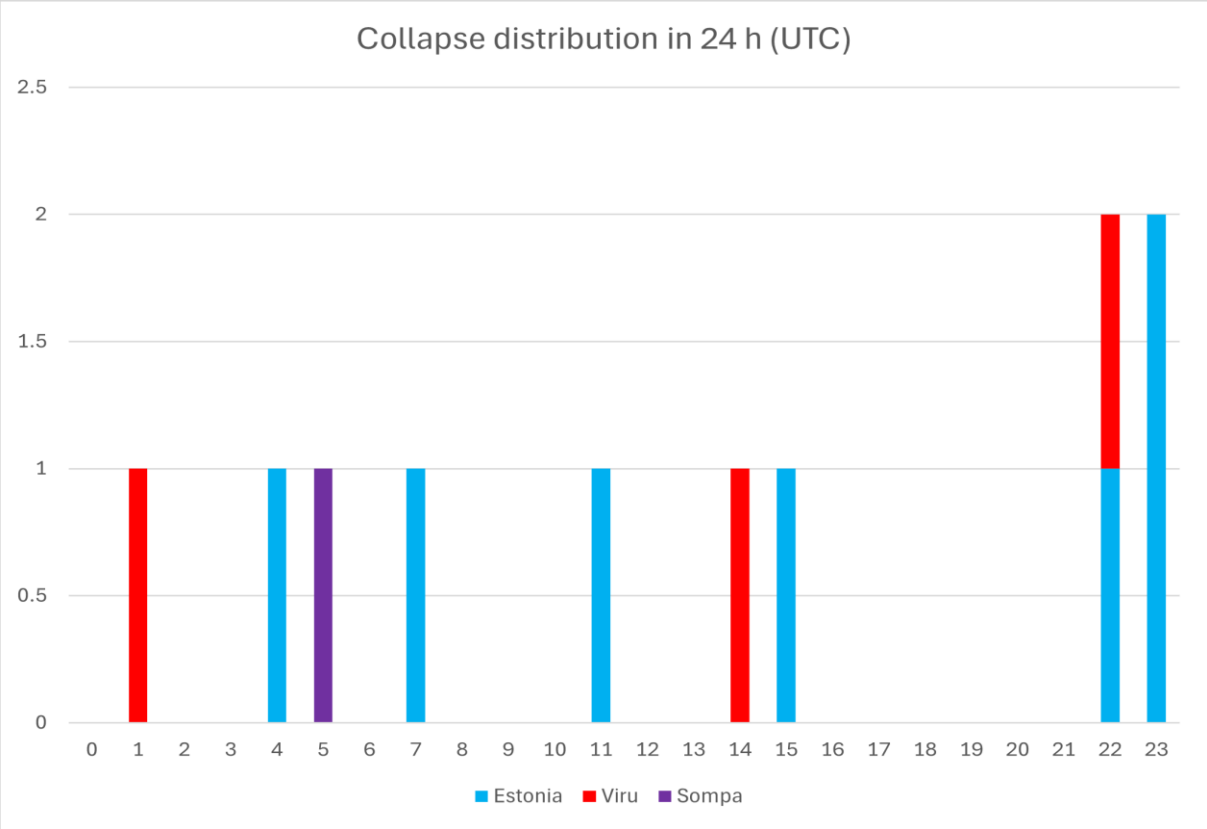

Figure 22. Times of day when collapses have occurred, in UTC time.

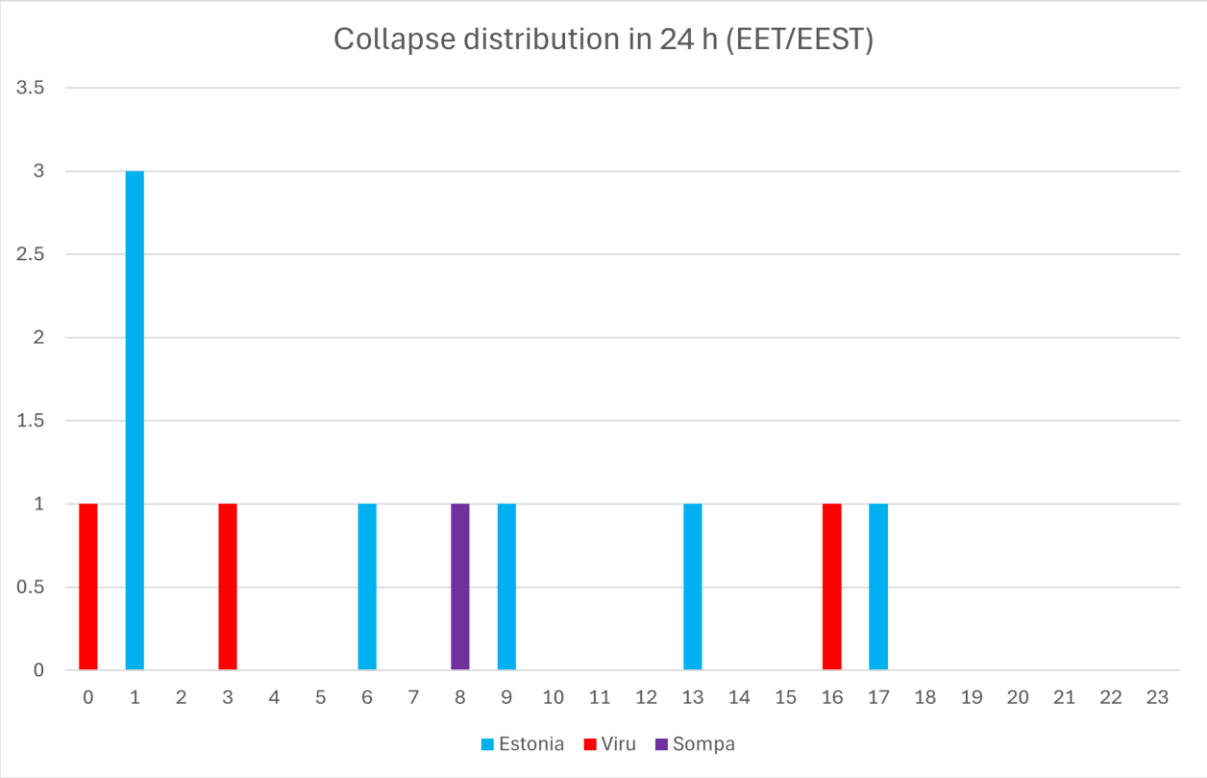

Figure 23. Times of day when collapses have occurred, in local EET/EEST time.

6.2. Meteorological conditions

Figure 24 illustrates the seasonal distribution of collapses. Winter and spring account for eight of the eleven collapses. I find it unlikely that summer conditions have held significant influence, the two cases of collapses being in 2008 in Estonia and 2016 in Sompa. The two collapses in 2008 took place in January and July, but their locations were very close to each other (see Appendix 3), suggesting that the circumstances leading to instability may have been the same or similar, perhaps to do with a single section of roof or adjacent pillars giving out. The collapse in Sompa occurred on June 7th but it was likely more related to the 2016 years unusual weather patterns compared to previous and following years.

Winter and spring have far more influential weather conditions, such as snow, meltwater and rain. The years 2015–2016 experienced unusual shifts in weather conditions compared to historic records. Winter and spring in 2015 were 2–4° warmer than usually (Estonian Environment Agency, 2016) and 2016 experienced warmer temperatures (+3°C) as well as high precipitation totals (up to 157% of normal) from winter to mid-summer (Estonian Environment Agency, 2015). This was also a period when freeze-thaw cycles shifted from April and May to March (Jaagus et al., 2017), increasing snowmelt and rainfall in early spring. Such conditions are significant because water may play a critical role in increasing the chances of collapses occurring. When water enters microfractures in rock and freezes due to low temperatures, the fractures are further expanded, thus weakening the rock. Meltwater and rain also increase the levels of groundwater and hydraulic pressure in overburden layers and, as discussed in earlier chapters, groundwater levels considerably effect conditions in an underground mine.

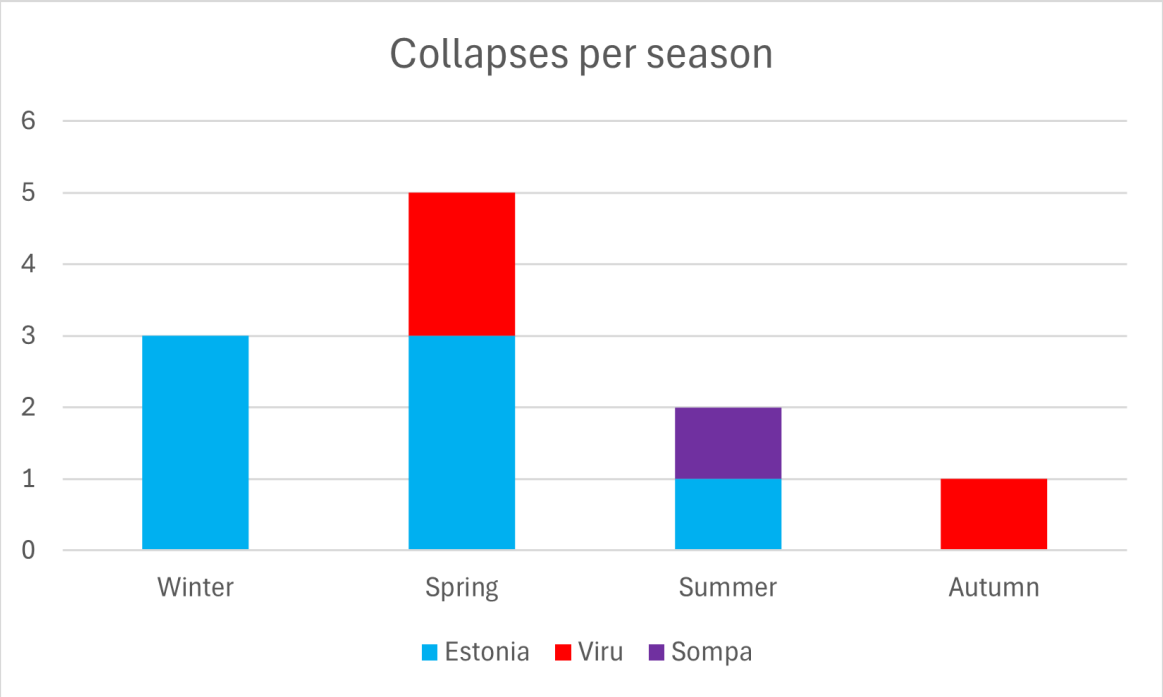

Figure 24. Number of collapses that took place in each season.

6.3. Location

An important factor is geographical and geological locations of the collapses. Figure 25 shows a density map of collapses per km^2 in the mine areas. Approximate calculations showed that of the total area, collapses occupy around 7.3%, with the average number of events per km^2 being less than 0.05. Though these numbers are quite small, there seems to be a pattern that the collapses follow, forming a line through the three mines in a south-east direction with few deviations. I also compiled a map (Figure 26, and the same map in higher resolution in Appendix 3) of the area that shows the locations of all the 11 collapses with their respective sources (both seismically determined and physically located in the landscape), known areas of ground subsidence and geological features such as faults and karst zones. This map gives a promising overview of how collapses and geological features seem to be located with a certain alignment. Many karst zones appear at the borders of the mines and so do the collapses. The collapses at Sompa and Viru are especially well aligned, which prompted me to try the signal stacking exercise described in chapter 5.3. The 2023 collapse at Estonia, which is one of two deviations from the general location alignment, likely occurred – at least to a certain extent – due to the added weight of a solar power plant being built on the premises (Soosalu, 2024). A more precise mapping of which mining technologies and structural reinforcement methods were used during each year any collapse occurred may provide even further correlating conditions that ultimately led to these structural failures.

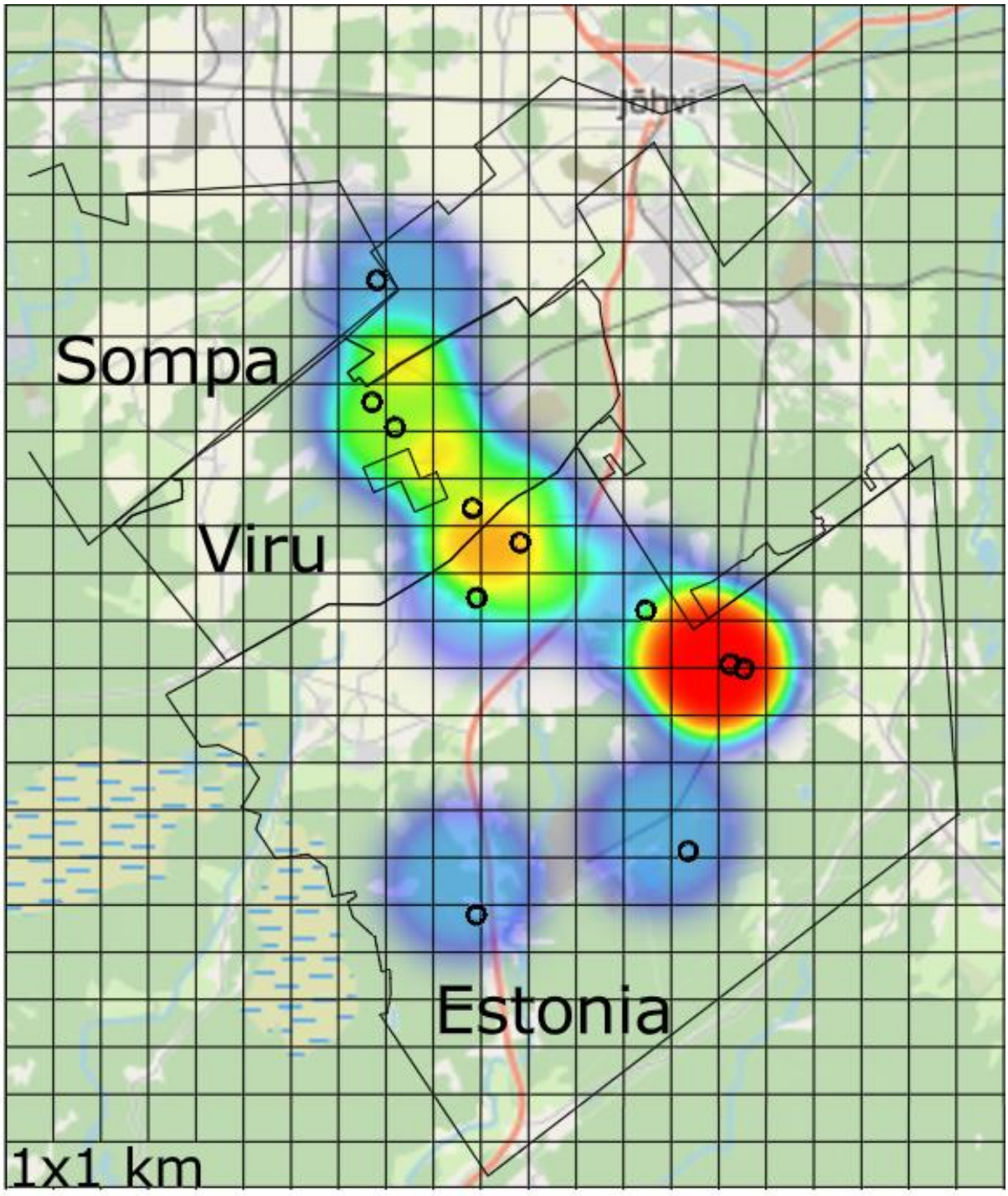

Figure 25. Collapses per km^2 represented by black circles and coloured by event density.

The event density scale: blue – a single event per km^2, green – single events in proximity, red – two events per km^2.

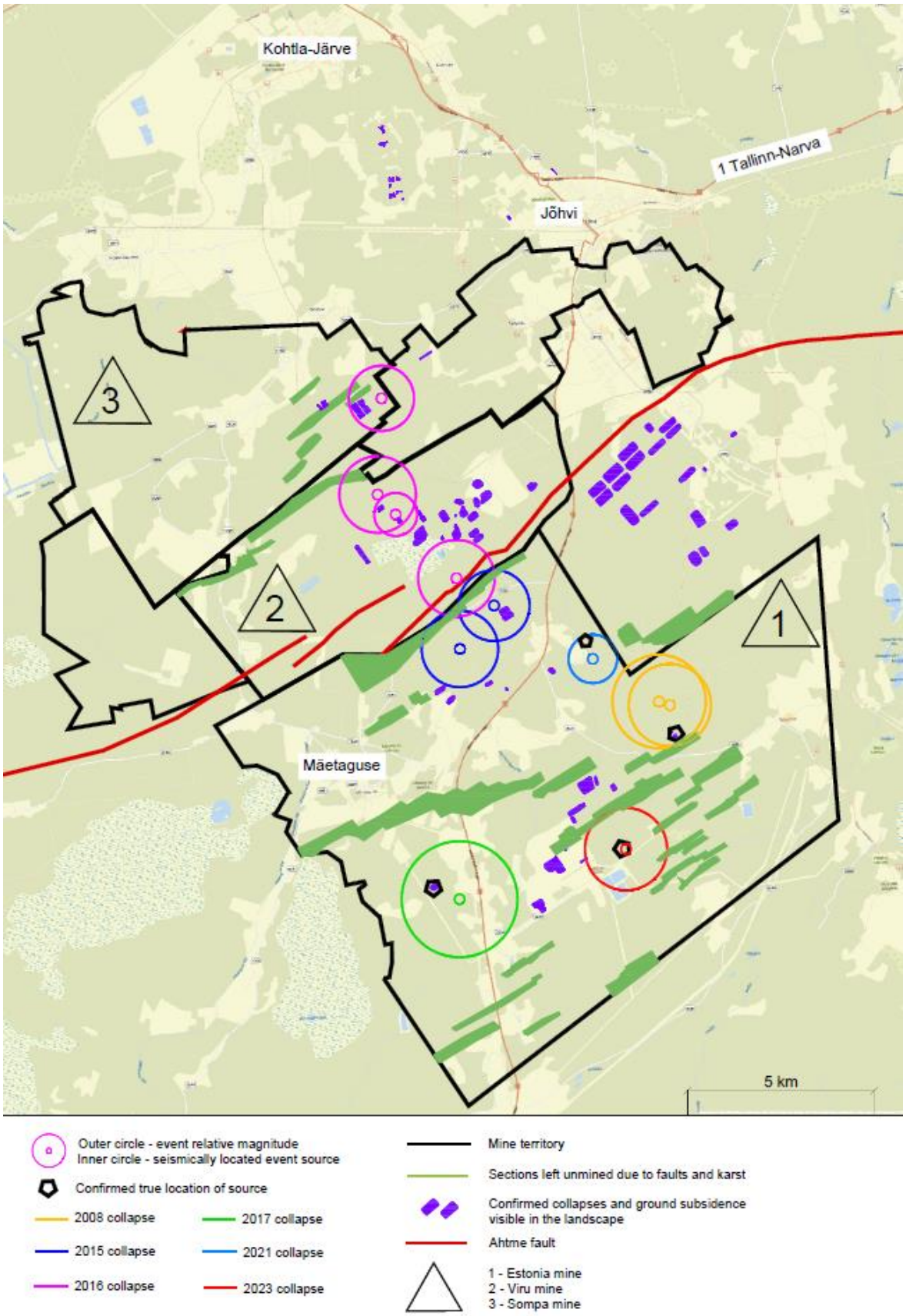

Figure 26. An overview of the oil shale mining region under analysis. The map was made using Autodesk Civil 3D.

7. Conclusions and Discussion

The primary objective of this thesis was to investigate the causes and conditions surrounding underground collapses in oil shale mines in northeastern Estonia. Through analysis of seismic records collected between 2008 and 2023, signal processing techniques and geological context, this study aimed to identify patterns and possible predictive factors contributing to the occurrence of collapses in the mines Estonia, Viru and Sompa. Comparisons of seismic events and waveform analysis showed how underground collapses differ from other types of events, such as earthquakes and explosions. Collapses are characterized by uniquely longer and lower frequency signals, possibly caused by seismic energy resonating within mine cavities, much like sound in a musical instrument. Identifying collapses early through seismological observations helps to locate potentially hazardous surface openings in the landscape, often leading to collapses that may have otherwise gone unnoticed.

Among these eleven collapses, distributional patterns related to time and location emerged. Time dependant correlations included collapse rates increasing in winter and spring, specific days of the week and night-time hours, when ventilation is halted and conditions such as temperature and humidity change. Seasonal preferences point to the effects of meteorological conditions, most notably freeze-thaw cycles and rainfall. In the case of the years 2015–2016, high precipitation totals and a shift in snowmelt maximums to an earlier month seemed to coincide with collapses becoming more frequent, suggesting that water may have a significant effect on the structural integrity of a mine even if it has remained stable for an extended period. Groundwater is also related to the formation of karst zones, which are a considerable hindrance to mining operations due to the instability they cause in rock layers.

While several correlating factors of collapses were presented and considered, definitive conclusions are limited. The seismic stations network had less stations in the years prior to 2015, meaning smaller events may have gone undetected. Further refinement and inclusion of more stations will provide more accurate results in the future.

Summary

This thesis explored the mechanisms and contributing conditions of underground collapses in the oil shale mining region in Estonia. The study aimed to determine whether these collapses could be linked to identifiable patterns or conditions such as mining activity, geological features, time and seasonal or meteorological changes. Primary tasks in the research included comparing signals of different types of seismic events using Python-based filtering and visualization, stacking seismic signals to enhance data clarity and analyzing collapses in the context of time, weather conditions, geological location and mining methods.

The results highlight how mine collapses are distinguishable from other seismic events based on their unique waveform characteristics. Collapse occurrence patterns suggest that events are more common during the night and in winter and spring, implicating the significance of changes in environmental, specifically hydrological, and operational conditions. Geological mapping indicated that collapses may coincide with features like faults and karst zones, as they often compromise mining structures. In conclusion, the study highlights that collapses may result from a combination of environmental stressors and structural weaknesses. Seismological monitoring is a critical tool in locating and possibly predicting collapses in order to ensure environmental safety, both above and below the surface.

Acknowledgements

I would like to express my deepest gratitude to my supervisor, Heidi Soosalu, for introducing me to this fascinating research topic and for guiding me through the process of practicing seismic data analysis. Her expertise and encouragement were crucial in helping me understand seismology as a precise and complex field of research. I am grateful for her thoughtful advice on academic writing as well. I would also like to sincerely thank professor Savka Dineva of Luleå University of Technology for providing a thorough introduction to seismology, with a focus on mining-induced seismicity. Her teaching helped me become familiar with the fundamentals of seismicity and seismic data processing, both in domestic mining environments and in international contexts. I am thankful to have learned so much from such experienced mentors and hope to return to this field in the future.

References

Dyni, J., R. (2006). Geology and Resources of Some World Oil-Shale Deposits. U.S. Geological Survey. https://pubs.usgs.gov/sir/2005/5294/pdf/sir5294_508.pdf

Estonian Environment Agency. (2016). *Weather events in 2016*. https://www.ilmateenistus.ee/kliima/weather-events/2016-2/?lang=en

Estonian Environment Agency. (2015). *Weather events in 2015*. https://www.ilmateenistus.ee/kliima/weather-events/2015-2/?lang=en

Institute of Seismology, University of Helsinki (1980): The Finnish National Seismic Network. GFZ Data Services. Dataset/Seismic Network. doi:10.14470/UR044600

Iannacchione, A. T., Esterhuizen, G. S., Bajpayee, T. S., Swanson, P. L., & Chapman, M. C. (2005). Characteristics of mining-induced seismicity associated with roof falls and roof caving events. Proceedings of the 40th U.S. Rock Mechanics Symposium.

Jaagus, J., Sepp, M., Tamm, T., Järvet, A., & Mõisja, K. (2017). Trends and regime shifts in climatic conditions and river runoff in Estonia during 1951–2015. *Earth System Dynamics, 8*(4), 963–976. https://esd.copernicus.org/articles/8/963/2017/index.html?utm_source=chatgpt.com

Kattai, V., Saarde, T., & Savitski, L. (2000). *Eesti põlevkivi*. Geological Survey of Estonia.

Kattai, V. (2001) *Seletuskiri Viru kaevevälja põlevkivivaru ümberhindamise kohta (varu seisuga 01.01.2001)*. Eesti Geoloogiakeskus. https://fond.egt.ee/fond/egf/7235

Kattai, V. (2003). *Põlevkivi – Õlikivi*. Geological Survey of Estonia.

Koit, O. (2018). Distribution and development conditions of karst phenomena in Estonia. *Dynamiques environnementales, 42,* 292–299. https://doi.org/10.4000/dynenviron.2253

Larsson, K. (2004). *Mining induced seismicity in Sweden*. [Licentiate thesis, Luleå University of Technology]. https://www.diva-portal.org/smash/record.jsf?pid=diva2%3A990731&dswid=5782

Meidla, T., Ainsaar, L., & Hints, Olle. (2014). The Ordovician System in Estonia. Field Guide, 74th Annual Meeting of IGCP 591. https://www.researchgate.net/publication/312948281_The_Ordovician_System_in_Estonia

ObsPy. A Python Framework for Seismology. (i.a). ObsPy Documentation (1.4.2). https://docs.obspy.org/

Orlik, N. (2009). *Taotlus Eesti Energia Kaevandused AS Viru kaevevälja karstialade põlevkivivaru mahaarvamise kohta (varu seisuga 01.01.2009. a)*. Eesti Energia Kaevandused AS https://fond.egt.ee/fond/egf/8202

Ottemöller, L., & Havskov, J. (2010). *Routine data processing in earthquake seismology: With sample*

data, exercises and software. Springer.

Pandivere kõrgustik. (n.d.). Eesti Entsüklopeedia. http://entsyklopeedia.ee/artikkel/pandivere_kõrgustik1

Raudsep, R. (2008). Estonian georesources in the European context. *Estonian Journal of Earth Sciences, 57,* 80–86. http://dx.doi.org/10.3176/earth.2008.2.03

Reinsalu, E. (2011). *Eesti mäendus*. Tallinn University of Technology.

Reinsalu, E., Toomik, A., & Valgma, I. (2015). *Kaevandatud maa*. Tallinn University of Technology, Department of Mining. https://digikogu.taltech.ee/et/item/0b841e2d-6128-41e0-a065-184afe2a3b4d

Seismic Events in Northern Europe. (n.d.). Final monthly bulletins. Institute of Seismology, University of Helsinki. https://www.seismo.helsinki.fi/bulletin/list/pdfbul.html

Soosalu, H. (2009). *Seismiline seire. Aruanne riikliku keskkonnaseire allprogrammi "Seismiline seire" täitmisest 2008. aastal*. Eesti Geoloogiateenistus. https://fond.egt.ee/fond/egf/8046

Soosalu, H. (2018). *Seismiline seire. Aruanne riikliku keskkonnaseire allprogrammi "Seismiline seire" täitmisest 2017. aastal*. Eesti Geoloogiateenistus. https://fond.egt.ee/fond/egf/8873

Soosalu, H. (2021). *Seismiline seire. Aruanne riikliku keskkonnaseire allprogrammi "Seismiline seire" täitmisest 2020. aastal*. Tallinna Tehnikaülikool, Geoloogia Instituut. https://fond.egt.ee/fond/egf/9457

Soosalu, H. (2024). *2023. aasta seismiline seire. Aruanne*. Eesti Geoloogiateenistus. https://fond.egt.ee/fond/egf/9836

Soosalu, H. (2025). *2024. aasta seismiline seire. Aruanne*. Eesti Geoloogiateenistus. https://fond.egt.ee/fond/egf/9948

Soosalu, H., & Valgma, I. (2009). Seismoanalüüsiga võib tuvastada kaevandusvaringuid. *Keskkonnatehnika*, 3, 6–9.

Stein, S., & Wysession, M. (2003). *An introduction to seismology, earthquakes, and earth structure*. Blackwell Publishing.

Triton, L., Earle, S., Bačić, M., Librić, L., Kaćunić, D. J., & Kovačević, M. S. (2023). Body waves and surface waves. Wikimedia Commons. https://commons.wikimedia.org/wiki/File:Overview_Seismic_Waves.jpg

Wang, J.-A., Shang, X.C., Ma, H.T. (2008). Investigation of catastrophic ground collapse in Xingtai gypsum mines in China. *International Journal of Rock Mechanics and Mining Sciences, 45*(8), 1480–1499. https://doi.org/10.1016/j.ijrmms.2008.02.012

Vassiljev, J., Aarniste, M., Rebane, K., & Urtson, K. (2018). *Põlevkivi altkaevandatud alade varingute*

uuring (KIK Project nr. 11735). Tallinn University of Technology, Institute of Geology. https://fond.egt.ee/fond/egf/8911

Viil, A. (2020). *Enefit Kaevandused AS Estonia kaevevälja karstialade põlevkivivaru bilansist mahaarvamise kohta (varud seisuga 01.01.2020)*. Enefit Kaevandused AS. https://fond.egt.ee/fond/egf/9428

Viil, A., & Orlik. N. (2014). *Taotlus Eesti Energia Kaevandused AS Viru kaevevälja karstialade põlevkivivaru bilansist mahaarvamise kohta (varud seisuga 01.04.2013. a)*. Eesti Energia Kaevandused AS. https://fond.egt.ee/fond/egf/8560

Viirland, A. (2000). *Seletuskiri Sompa kaevevälja põlevkivivarude ümberhindamise (seisuga 01.11.2000) taotlusele*. AS Estonia Kaevandus. https://fond.egt.ee/fond/egf/7101

Appendix 1. An example Python code used to plot seismic data

```
from obspy import read  # Reads seismic data files such as MiniSEED)

import matplotlib.pyplot as plt  # Used for plotting graphs


st = read ("2016064012300ARBE.mseed")  # Load the MiniSEED file

#print(st)  # Optional: Prints metadata of all traces (Z, N, E), including station, channel, start time, sampling rate, etc

st.sort(keys=["channel"])  # Sorts the traces based on their channel name


st.filter("bandpass", freqmin=0.8, freqmax=10)  # Applies a bandpass filter to remove noise outside the 0.8-10 Hz frequency range

#st.filter("highpass", freq=0.8)  # Applies a highpass filter to remove frequencies below 0.8 Hz


st.plot(equal_scale=False)  # Plots all traces with separate amplitude scale


z_trace= next(tr for tr in st if tr.stats.channel[-1].upper() == "Z")  # Selects the Z-component trace

fig = z_trace.spectrogram(log=True, wlen=10, show=False, title="Z-Component")  # Plots a spectrogram of the Z-component


ax = fig.axes[0]  # Accesses the first axis in the figure

ax.set_ylim(0.5, ax.get_ylim()[1])  # Adjusts the Y-axis limits of the spectrogram; lower limit is set to 0.5 Hz

plt.show()  # Displays all plots
```

Appendix 2. An example of an output file of the routine seismic analysis of Estonian events, featuring the collapse in the Estonia mine in December 2023 (from Soosalu, 2024).

Output of the location program. The time is UTC (EET-2 hours) (table format: http://www.seismo.helsinki.fi/bulletin/list/nordic_format.html).

```
2023 1224 0453 52.2 LI 59.207  27.415  0.0F HEL 31 0.3 1.6LHEL                1
GAP=124         0.1     0.325   0.360                   0.1                    5
COLLAPSE, ESTONIA MINE NORTHEASTERN ESTONIA, CONFIRMED                         3
CSS:2023358045310.WFDISC                                                       6
STAT SP IPHASW D HRMM SECON CODA AMPLIT PERI AZIMU VELO SNR AR TRES W  DIS CAZ7
EE04 BZ EP         453 57.23                                    -0.210   32  54
EE04 BZ ES         454  0.92                                    -0.2 5
TOSE CE EP         454  3.88                                    -0.5 7   76 241
TOSE CN ES         454 14.11                                     1.0 0
ARBE HZ EP         454  6.28                                     0.3 9   86 288
ARBE HZ ES         454 15.95                                     0.1 5
VSU  HZ EP         454  7.11                                     0.1 9   92 206
VSU  HN ES         454 17.31                                    -0.3 4
SRGE CZ EP         454 14.52                                    -0.2 8  140 245
SRGE CZ ES         454 30.72                                    -0.0 4
SRGE CZ ESN        454 35.59                                     0.8 1
VJF  HZ EPB        454 16.46                                     0.2 8  149   3
VJF  HZ ESB        454 33.87                                     0.2 4
VJF  HZ  MSG       454 39.10        5.55 0.18
LOVF CZ EPB        454 16.92                                     0.3 8  152 336
LOVF CZ ES         454 34.14                                     0.1 4
LOVF CZ  MSG       454 35.68        5.78 0.20
PISE CZ EP         454 16.86                                     0.1 3  152 179
PISE CE ES         454 34.80                                     0.5 8
PISE CZ  MSG       454 39.93        8.37 0.19
EE02 BZ EP         454 17.34                                     0.1 3  156 270
EE02 BZ ES         454 34.87                                    -0.3 8
VUOS BZ EP         454 19.32                                     0.1 2  169 312
VUOS BZ ES         454 38.18                                    -0.6 8
VUOS BZ  MSG       454 41.77        3.72 0.23
PVF  CZ EPG        454 20.28                                     0.2 8  173 330
PVF  CZ ES         454 39.34                                    -0.6 4
LAUT BZ EPN        454 21.43                                    -0.2 4  179 307
LAUT BZ ESG        454 41.92                                     0.3 8
LAUT BZ  MSG       454 43.86        3.27 0.19
HEL1 BZ EPN        454 21.78                                     0.1 7  179 308
HEL1 BZ ES         454 41.36                                    -0.3 2
RSUO BZ EPN        454 21.73                                    -0.1 8  180 309
RSUO BZ ESG        454 42.07                                     0.2 4
HEL5 BZ EPN        454 21.97                                    -0.1 8  182 305
HEL5 BN ESG        454 43.00                                     0.5 4
KUNI BZ EP         454 21.27                                    -0.3 8  184 311
KUNI BZ ESN        454 44.45                                     0.1 4
KUNI BZ  MSG       454 46.58        3.68 0.19
KY17 CZ EP         454 23.06                                     0.0 8  194 354
KY17 CZ ESN        454 46.44                                    -0.1 4
MEF  BZ EPG        454 25.34                                     0.2 7  204 305
MEF  BZ ES         454 47.41                                    -0.7 3
MEF  BZ  MSG       454 50.11        4.02 0.19
NUR  SZ EPG        454 26.86                                     0.4 4  213 314
NUR  SZ ES         454 49.98                                    -0.3 6
NUR  SZ  MSG       454 52.44        5.27 0.25
MTSE HZ EPG        454 26.78                                    -0.0 3  215 257
MTSE HZ ES         454 51.03                                     0.2 5
NOPE CZ EP         454 26.47                                     0.1 4  217 272
NOPE CZ ES         454 51.60                                     0.2 6
IMAF CZ EP         454 28.68                                     0.1 7  235  20
IMAF CZ ESG        454 56.84                                    -0.2 3
TVF  BZ EPB        454 31.29                                     0.4 6  247 288
TVF  BZ ESG        454 59.86                                    -0.5 1
TVF  BZ  MSG       455  1.97        2.01 0.16
FIA0 HZ EP         454 31.37                                    -0.4 3  260 344
FIA0 HZ ESG        455  4.04                                    -0.1 0
FIA1 HN EP         454 31.30                                    -0.5 0  260 344
FIA1 HZ ESG        455  4.00                                    -0.1 1
RUF  BZ EPB        454 33.26                                     0.2 0  262  18
RUF  BN ESB        455  3.37                                     0.3 0
EE06 BZ ESG        455  4.54                                    -0.4 0  263 266
KAF  HZ EP         454 40.85                                     0.4 0  330 350
KAF  HN ES         455 16.55                                     0.8 0
KAF  HZ  MSG       455 23.99        2.13 0.22
SLIT HN ESG        455 26.52                                    -1.2 0  346 242
AAL  BZ EPG        455  3.04                                     1.1 0  432 288
AAL  BZ ESG        455 52.24                                     0.7 0
AAL  BZ  MSG       455 54.65        1.88 0.27
JOF  BZ EP         454 56.96                                    -0.3 0  465  25
```

Appendix 3. A map with all collapses and where they occurred in the oil shale mines. Shown in Figure 26 and in a separate file on a magnified scale.

The map was made using spatial data from the Estonian Geoportal Web Maps Geological Data 1:50 000, Geological Data 1:40 000 and Mineral Deposits:
https://xgis.maaamet.ee/xgis2/page/app/maardlad

Also, used were reports on re-evaluations of oil shale reserves due to karst areas of the mining field from the Viru, Sompa and Estonia mines (Viil, 2020), (Viirland, 2000), (Kattai, 2001), (Viil & Orlik, 2014), (Orlik, 2009).

Lisa
rektori 07.04.2020 käskkirjale nr 1-8/17

Lihtlitsents lõputöö reprodutseerimiseks ja lõputöö üldsusele kättesaadavaks tegemiseks[1]

Mina _____ (a*utori nimi*)

1. Annan Tallinna Tehnikaülikoolile tasuta loa (lihtlitsentsi) enda loodud teose
_____
_____
_____,
(*lõputöö pealkiri*)

mille juhendaja on _____,
(*juhendaja nimi*)

1.1 reprodutseerimiseks lõputöö säilitamise ja elektroonse avaldamise eesmärgil, sh Tallinna Tehnikaülikooli raamatukogu digikogusse lisamise eesmärgil kuni autoriõiguse kehtivuse tähtaja lõppemiseni;

1.2 üldsusele kättesaadavaks tegemiseks Tallinna Tehnikaülikooli veebikeskkonna kaudu, sealhulgas Tallinna Tehnikaülikooli raamatukogu digikogu kaudu kuni autoriõiguse kehtivuse tähtaja lõppemiseni.

2. Olen teadlik, et käesoleva lihtlitsentsi punktis 1 nimetatud õigused jäävad alles ka autorile.

3. Kinnitan, et lihtlitsentsi andmisega ei rikuta teiste isikute intellektuaalomandi ega isikuandmete kaitse seadusest ning muudest õigusaktidest tulenevaid õigusi.

_____ (kuupäev)

_____

[1] *Lihtlitsents ei kehti juurdepääsupiirangu kehtivuse ajal vastavalt üliõpilase taotlusele lõputööle juurdepääsupiirangu kehtestamiseks, mis on allkirjastatud teaduskonna dekaani poolt, välja arvatud ülikooli õigus lõputööd reprodutseerida üksnes säilitamise eesmärgil. Kui lõputöö on loonud kaks või enam isikut oma ühise loomingulise tegevusega ning lõputöö kaas- või ühisautor(id) ei ole andnud lõputööd kaitsvale üliõpilasele kindlaksmääratud tähtajaks nõusolekut lõputöö reprodutseerimiseks ja avalikustamiseks vastavalt lihtlitsentsi punktidele 1.1. jq 1.2, siis lihtlitsents nimetatud tähtaja jooksul ei kehti.*